Submitted to Physical Review B

LBL-6942
Preprint

ALFVÉN-WAVE OSCILLATIONS IN A SPHERE, WITH APPLICATIONS TO ELECTRON-HOLE DROPS IN Ge

R. S. Markiewicz

January 1978

Prepared for the U. S. Department of Energy
under Contract W-7405-ENG-48

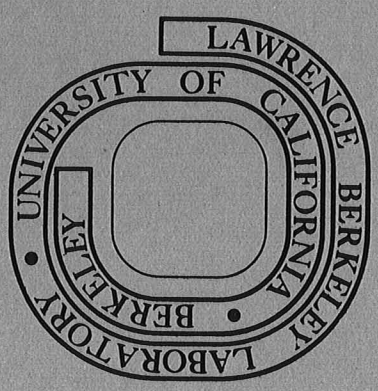

Submitted to Physical Review B

LBL-6942

ALFVÉN-WAVE OSCILLATIONS IN A SPHERE, WITH APPLICATIONS TO ELECTRON-HOLE DROPS IN Ge*

R. S. Markiewicz†

Physics Department,
University of California,
Berkeley, California 94720

and

Materials and Molecular Research Division,
Lawrence Berkeley Laboratory,
Berkeley, CA 94720

(received Jan. 1978)

ABSTRACT

The problem of Alfvén-wave oscillations in an anisotropic sphere is studied, and two solutions are presented. One solution is exact, involving an expansion of the current inside the sphere in a series of orthonormal modes. The second is approximate, based on a perturbation expansion of the induced fields and currents in powers of the drop radius. The approximate solution can be applied to a material having a completely general conductivity tensor, while the exact solution is restricted to situations of high symmetry.

As an illustration of these solutions, the resonant power absorption by electron-hole droplets in Ge is calculated explicitly. Size-dependent resonances, for which the resonant field increases with the drop radius, have been observed experimentally. The present calculation

*Supported in part by the U.S. Energy Development and Research Administration.

†Present Address: Physical Science Branch, General Electric Co., Corporate Research and Development, Schenectady, NY 12345.

shows that such resonances occur both in the magnetic and electric dipole absorption, with the magnetic dipole absorption being most intense, particularly for small drops. From the approximate solution, it is found that certain of the resonances can have a very strong dependence on the orientation of the magnetic field with respect to the crystal axes, similar to cyclotron resonance of an electron in Ge.

As a second application of these results, the transition from Alfvén waves (in a material having equal numbers of electrons and holes) to helicon waves (only one carrier type) is studied. The "elimination" of one carrier type can be accomplished by increasing its mass, decreasing its concentration, or increasing its collision rate. The Alfvén to helicon transitions are quite different in each of these three cases, and examples of intermediate states are presented.

I. INTRODUCTION

A. Scattering of Waves by a Sphere

Electromagnetic waves have long been a valuable probe of the properties of free carriers in solids. A particularly important technique in semiconductors has been cyclotron resonance:[1] this gives the effective mass m and (using circularly polarized waves) the sign of the charge for each type of carrier in the material. From the linewidths, information can be found concerning collision processes of the carriers. Unfortunately, this technique can generally only be used when the number of carriers is small.[2] A high density n of carriers screens out low-frequency electric fields, and shifts the cyclotron resonance to frequencies near the plasma frequency,[3]

$$\omega_p = (4\pi ne^2/\varepsilon_L m)^{1/2} \qquad (1)$$

where ε_L is the dielectric constant of the medium. The remaining plasma resonances and plasma-shifted cyclotron resonance contain much less information than the cyclotron resonance. The peak gives a measure only of the ratio n/m, and if these are several types of carriers, the effective mass is an average among those types.

A static magnetic field B greatly changes the situation, opening a "window" in the normally screened frequencies below the plasma frequency: certain low-frequency waves can propagate through the material without loss if their frequency ω is less than the cyclotron

frequency,

$$\omega_c = eB/mc \qquad (2)$$

The nature of these waves depends sensitively on the types of carriers in the material.[4] For a material with a single type of carrier, the propagating waves, called helicons, have one sign of circular polarization (depending on the sign of the carrier's charge) and are highly dispersive, $k \propto \omega^{1/2}$, where $k = 2\pi/\lambda$ is the wave number, and λ the wavelength in the medium. If there are equal numbers of electrons (negatively-charged carriers) and holes (positively-charged), then dispersionless, linearly-polarized waves can propagate. These are called Alfvén waves.

Such propagating waves can be conveniently studied using "dimensional resonance" techniques: by matching the linear dimension of a sample to the wavelength of the propagating wave, it is possible to excite a normal mode oscillation inside the solid, for which the absorption of the wave is greatly enhanced. This absorption is resonant in the wavelength of the wave (or the length of the sample). The technique therefore allows a precise measurement of the wavelength inside the sample, from which the properties of the carriers can be determined. The resonance condition is most easily visualized in a flat plate: the thickness of the plate t must be equal to an integral number, j, of half-wavelengths: $t=j\lambda/2$. Such resonances are by no means confined to flat plates. Figure 1 shows schematically the field distributions in a sphere near the lowest two (dipole) dimensional resonances. (This figure will be

discussed in more detail later on) Below the spheres are shown the intensity of the electric fields at different points along the sphere diameter. The sinusoidal pattern clearly indicates what is meant by fitting one (or two) wavelengths inside the sphere. For a sphere of radius a, the resonance condition can be written $2\pi a = \gamma_{ij}\lambda$, or

$$ka = \gamma_{ij} \tag{3}$$

Here the γ_{ij} are a series of constants which, for the slab, would be πj. For the sphere, these constants are to be found by solving the electromagnetic boundary value problem for absorption by a sphere. This difficult problem is the central topic of this paper.

In a magnetic field, λ is a function of B, so that the absorption is also resonant in B. As B is varied, a series of resonances will appear, different resonances associated with different normal modes (γ_{ij}). When a is varied, the peaks of these resonances, B_r, will shift in a characteristic manner which is different for helicon waves ($B_r \propto a^2$) and Alfvén waves ($B_r \propto a$). This is discussed further in Section II.

If the conductivity of the sphere is an isotropic scalar, then the problem reduces to Mie scattering,[5] for which the solutions are well known, and will serve in this paper as a guide to the more general problem. Unfortunately, in the problem of interest, the magnetic field breaks the spherical symmetry and introduces a tensor conductivity. The problem of electromegnetic scattering in this case remained unsolved for almost fifty years. Recently, Ford and Werner[6] presented a formally exact numerical technique to calculate the magnetic dipole absorption

in this problem, in the special case in which there is a single carrier type with scalar mass. This solution places some limit on the size of the sphere, but in practice it is not very restrictive. The sphere must be small compared to the wavelength outside the sphere. The wavelength inside the sphere is reduced by $\sqrt{\varepsilon}$, where ε is the effective dielectric constant of the medium (given, e.g., by Eq. (6) below). For a good conductor in a magnetic field, this reduction can be of the order of 100. In the specific example of this paper - electron-hole drops in Ge - the drops were probed with K-band microwaves, so that the wavelength outside the drop is 3 mm - much larger than the largest drops observed.

B. Electron-hole Drops in Ge

In a recent series of experiments,[7,8] such dimensional resonances have been observed in microwave absorption by electron-hole drops (EHD) in Ge.[9] These drops are produced by condensation of excitons at low temperatures, and in unstrained Ge form small ($a \sim 2$-10 μm)[10] metallic spheres, having equal numbers of electrons and holes, and a pair density of about 2.3×10^{17} cm^{-3}. From an approximate theory of the dimensional resonances[7,11] (briefly described in Section II e below), a drop radius $a > 100$ μm was estimated, suggesting that what was observed was not the ordinary, small EHD. Subsequent experiments[9,12,13] confirmed that the sample was strained in such a way as to produce a potential well[12,14] inside the sample, and that the small EHD were all attracted into the well, forming a single large mass of electron-hole liquid (EHL) near the bottom of the well. Because of the large strains,

the properties of this large liquid mass - called a γ-drop - are quite different from the properties of EHD in unstressed Ge. The pair density is considerably lower, $n = 5 \times 10^{16}$ cm^{-3},[15] and consequently the recombination lifetime is over an order of magnitude longer.

The purpose of the present paper is to extend the calculation of Ford and Werner to account for the dimensional resonances observed in these γ-drops. The calculation is complicated because there several carrier types with anisotropic masses. In unstressed Ge the conduction band consists of four equivalent electron valleys with ellipsoidal masses symmetric about the different ⟨111⟩-axes of the crystal: $m_\ell = 1.58\ m_0$, $m_t = 0.082\ m_0$,[1] where m_0 is the free electron mass. Under a large ⟨111⟩-stress (as is associated with γ-drops[14]), three of the valleys are raised in energy and only a single one remains populated. The valence bands consist of two warped hole bands, which are also gradually split by a ⟨111⟩-stress. Further details of these bands are presented in Appendix I. Thus, application of ⟨111⟩ stress gives rise to three distinct types of EHL: Ge(4:2), corresponding to very low (or zero) stress, for which 4 conduction band valleys and 2 valence bands are occupied; Ge(1:2), with 1 occupied conduction valley, but still 2 valence bands; and Ge(1:1), for large enough stress that only 1 valence band is occupied. The γ-drop corresponds to Ge(1:2), but the formal solution will also be applied to Ge(4:2) and Ge(1:1).

In Section II of this paper, the electromagnetic equations are summarized, and some simple properties of Alfvén and helicon waves are reviewed. Also a simple theory of the dimensional resonances,

due to Cardone and Rosenblum[16] is presented. The theory, based on an ad hoc application of Mie theory to the problem, is here called the empirical Mie theory (EMT). Section III presents the generalization of the exact theory of Ford and Werner.[6] In addition to including the multiple, anisotropic-mass carriers of Ge, the Rayleigh limit (small a) is treated correctly, and electric as well as magnetic dipole absorption is calculated. Section IV presents an approximate analytic solution to the same problem, based on Ref. 18. This approximate solution complements the exact solution in many ways. It is much easier to handle and, while it lacks the rich, resonant structure of the full theory, it nevertheless reproduces the basic properties of the principal resonances with a reasonable accuracy. Furthermore, it is more versatile than the exact solution. The exact solution can only be applied in cases of high symmetry, when the conductivity has a particularly simple form. For the EHL in Ge, this means the solution can only be found when the field lies along the stress (⟨111⟩-)axis, except in unstressed Ge, where solutions can be found if B is parallel to either a ⟨111⟩- or a ⟨100⟩-axis. In this paper, the approximate solution is generalized to an arbitrary conductivity tensor, and as an application the full angle dependence of the dimensional resonances in the EHL is shown.

In Section V, these theories are applied to the EHL in Ge, and a detailed comparison of the exact and approximate theories (as well as the EMT) is carried out. It is found that there is a quite complex spectrum; while the most intense absorption is magnetic dipole (excited

by the microwave magnetic field), there are also electric dipole resonances which should also be experimentally observable. These are three series of magnetic resonances, depending on the polarization of the microwave magnetic field B_1 with respect to the static field B: LM, for $\vec{B}_1 \parallel \vec{B}$; and TM$^{\pm}$, for transverse fields ($\vec{B}_1 \perp \vec{B}$) circularly polarized in opposite senses. Correspondingly, there are three series of electric resonances, LE and TE$^{\pm}$. The spectra are much more complicated than expected from the EMT: the magnetic field induces a "mode mixing" which induces a contribution to the dipole absorption from resonances associated with <u>all</u> the multipole modes of Mie theory. It is found that these dimensional resonances can be of great value in analyzing the properties of the carriers: from the Rayleigh limit resonances the effective carrier masses can be found, while the shift of these resonances in field as a is varied allows a determination of the carrier density. Finally, the linewidth can be used to measure collision rates of the carriers. In a subsequent publication, the results of this paper will be compared to the experimentally observed Alfvén resonances in EHD.

Helicon and Alfvén waves are just two limiting cases in a spectrum of possible resonances. In Section VI the transition between these two limits is briefly explored. For convenience, the initial material is taken to be composed of equal numbers of electrons and holes, each of which has an isotropic mass. The transition from Alfvén to helicon-like behavior is carried out in three different ways, each time by reducing the effectiveness of the holes as carriers. This is done by alternately decreasing the number of holes, increasing the hole mass,

and increasing the hole scattering rate. In each case the final state is the same: the resonance, due solely to the electrons, has features entirely characteristic of helicon waves. However the nature of the transition is quite different in the three cases, and illustrations are given of the very different types of resonances associated with the intermediate states (neither pure helicon nor pure Alfvén).

II. BASIC EQUATIONS

A. The Electromagnetic Equations

In a medium characterized by a complex tensor conductivity $\overleftrightarrow{\sigma}$,

$$\vec{j} = \overleftrightarrow{\sigma} \cdot \vec{E} \quad , \tag{4}$$

Maxwell's equations have the form (for a plane wave $\vec{E}(t) = \vec{E}\, e^{-i\omega t}$)

$$\vec{\nabla} \cdot \vec{E} = 0 \tag{5a}$$

$$\vec{\nabla} \cdot \vec{B} = 0 \tag{5b}$$

$$\vec{\nabla} \times \vec{E} = \frac{i\omega \vec{B}}{c} \tag{5c}$$

$$\vec{\nabla} \times \vec{B} = \frac{4\pi}{c} \vec{j} - \frac{i\omega}{c} \varepsilon_L \vec{E} \equiv - \frac{i\omega}{c} \overleftrightarrow{\varepsilon} \cdot \vec{E} \tag{5d}$$

$$\overleftrightarrow{\varepsilon} \equiv \varepsilon_L \overleftrightarrow{I} - \frac{4\pi}{i\omega} \overleftrightarrow{\sigma} \tag{6}$$

where ε_L is the lattice dielectric constant, and $\overleftrightarrow{I}$ is the identity matrix. Equations (5c) and (5d) can be combined to give the fundamental wave equation

$$\vec{\nabla} \times (\vec{\nabla} \times \vec{E}) = \frac{\omega^2}{c^2} \overleftrightarrow{\varepsilon} \cdot \vec{E} \tag{7}$$

In addition to satisfying Maxwell's equations in each medium, there also exist boundary conditions which must be satisfied at the interface between two media. These conditions require continuity of $\vec{B}$, of the transverse components of $\vec{E}$, and the normal components of $\overleftrightarrow{\varepsilon} \cdot \vec{E}$.

B. The Conductivity Tensor

The properties of the medium are determined by its dielectric constant and its conductivity tensor. The conductivity tensor is in general found by solving Boltzmann's equation,[17] but if the system of carriers can be characterized by an energy-independent collision time, τ, the conductivity tensor may be found more easily from an equation-of-motion method. This derivation will be appropriate for a degenerate Fermi system, for which only the collision time at the Fermi level is important. If the current is carried by a single kind of carrier having charge e, density n, and effective mass tensor $\overleftrightarrow{m}$, then the equation for the average carrier drift velocity $\vec{v}$ is

$$\overleftrightarrow{m} \cdot \left(\frac{d\vec{v}}{dt} + \frac{\vec{v}}{\tau}\right) = e\left(\vec{E} + \frac{\vec{v}}{c} \times \vec{B}\right) \tag{8}$$

If the time dependence of the drift velocity is also taken as sinusoidal with frequency ω, then the current density $\vec{j} = ne\,\vec{v}$ can be found:

$$\vec{j} = \overleftrightarrow{\sigma} \cdot \vec{E} \tag{9}$$

$$\overleftrightarrow{\sigma} = \overleftrightarrow{\rho}^{-1} \tag{10a}$$

$$\overleftrightarrow{\rho} \cdot \vec{j} = [(1/\tau - i\omega)\overleftrightarrow{m} \cdot \vec{j} + \frac{e}{c}\vec{B} \times \vec{j}]/(ne^2) \tag{10b}$$

For a carrier with isotropic mass $\overleftrightarrow{m} = m\overleftrightarrow{I}$, $\overleftrightarrow{\sigma}$ becomes:

$$\overleftrightarrow{\sigma} = \begin{pmatrix} \sigma_1 & \sigma_2 & 0 \\ -\sigma_2 & \sigma_1 & 0 \\ 0 & 0 & \sigma_3 \end{pmatrix} \tag{11}$$

where

$$\sigma_1 = \sigma_0(1-i\omega\tau)/[(1-i\omega\tau)^2 + (\omega_c\tau)^2] \tag{12a}$$

$$\sigma_2 = -\omega_c\tau\ \sigma_0/[(1-i\omega\tau)^2 + (\omega_c\tau)^2] \tag{12b}$$

$$\sigma_3 = \sigma_0/(1-i\omega\tau) \quad . \tag{12c}$$

$$\sigma_0 \equiv ne^2\tau/m \ , \tag{13}$$

ω_c is given by Eq. (2), and the magnetic field is taken to be along the z-axis (σ_3).

The above tensor may be diagonalized by going to the complex coordinates $\hat{x}_\pm = \hat{x} \pm i\hat{y}$ (corresponding to circularly polarized plane waves). Then

$$\overleftrightarrow{\sigma} = \begin{pmatrix} \sigma_+ & 0 & 0 \\ 0 & \sigma_- & 0 \\ 0 & 0 & \sigma_3 \end{pmatrix} \tag{14}$$

with

$$\sigma_\pm = \sigma_1 \pm \sigma_2 = \sigma_o/[1 - i(\omega \pm \omega_c)\tau] \tag{15}$$

If there are several types of carriers, their conductivities are additive. We shall be particularly interested in the situation in which there are equal numbers of electrons and holes. The simplest example of such a "compensated plasma" would consist of two types of carriers with isotropic masses, m_1 and m_2. Each carrier would have a conductivity of the form of Eq. (11), and the total conductivity would therefore also be of the same form.

For systems having conductivities of the form of Eq. (11) (or, equivalently, of Eq. (14), the multipole absorption can be found exactly, as will be shown in Section III. For the EHL in Ge in an external magnetic field, the conductivity is more complicated, as discussed in the introduction and in Appendix I. The conductivity has the simple form of Eq. (11) only if the field lies along a high symmetry direction. For the magnetic field aligned along other directions, the dipole absorption can be approximately found by the methods of Section IV.

C. Helicon and Alfvén Waves in an Unbounded Medium

Particular solutions of Eq. (7) are transverse-polarized plane waves:

$$\vec{E} = \vec{E}_1 \, e^{i(\vec{k}\cdot\vec{r} - \omega\tau)} \tag{16}$$

$$\vec{k} \cdot \vec{E}_1 = 0 \tag{17}$$

$$-k^2 \vec{E}_1 = \frac{\omega^2}{c^2} \overleftrightarrow{\varepsilon} \cdot \vec{E}_1 \tag{18}$$

The waves corresponding to the eigenfunctions of this equation are (1) a wave linearly polarized along the magnetic field, for which

$$k_1^2 = \frac{\omega^2}{c^2} \left(\varepsilon_L - \frac{4\pi\sigma_3}{i\omega}\right) \tag{19}$$

and (2) circularly polarized waves propagating along the magnetic field, for which

$$k_\pm^2 = \frac{\omega^2}{c^2} \left(\varepsilon_L - \frac{4\pi\sigma_\pm}{i\omega}\right) \tag{20}$$

For a single carrier with isotropic mass, k_1 is independent of magnetic field, while, for high frequencies ($\omega\tau \gg 1$)

$$k_{\pm}^2 \approx \varepsilon_L \frac{\omega^2}{c^2} \left(1 - \frac{\omega_p^2}{\omega(\omega \pm \omega_c)}\right) \tag{21}$$

where the plasma frequency ω_p is defined by Eq. (1). In zero field, k_1, $k_{\pm}$ all reduce to the familiar result for a metal

$$k_0^2 = \varepsilon_L \frac{\omega^2}{c^2} \left(1 - \frac{\omega_p^2}{\omega^2}\right) \tag{22}$$

Thus for $\omega < \omega_p$, k_0 is imaginary, and no waves can propagate in the medium below its plasma frequency. In a finite magnetic field, the situation is radially changed. For $\omega_p \gg \omega_c$, ω,

$$k_{\pm}^2 \approx -\frac{\varepsilon_L \omega}{c^2} \frac{\omega_p^2}{\omega \pm \omega_c} \tag{23}$$

Thus, for one sign of circular polarization, $k^2 > 0$ if $|\omega_c| > \omega$. These propagating waves are called helicon waves. For $\omega_c \gg \omega$, their dispersion relation is given by

$$k \approx \frac{\omega_p}{c} \sqrt{\frac{\varepsilon_L \omega}{|\omega_c|}} = \frac{1}{c} \sqrt{\frac{4\pi nec\omega}{B}} \tag{24}$$

These waves are highly dispersive ($k/\omega \neq$ constant), and have a wavelength $\lambda = 2\pi/k$ which increases as the square root of the magnetic field.

There is a close connection between the sign of the circular polarization and the sign of the electric charge of the carriers, as far as cyclotron resonance or helicon wave propagation is concerned. Cyclotron resonance is associated with an infinity of the conductivity. From Eq. (15), σ_+ becomes infinite when $\omega_c = -\omega < 0$ - that is, if the carriers have a negative charge. Similarly, from Eq. (21), if $|\omega_c| > \omega$, then k_+ is real if $\omega_c < 0$: in both cases, the (+)-polarized wave is helicon-or cyclotron-active for negatively charged particles. The opposite result holds for the (-)-polarized wave.

In a compensated plasma, containing two types of carriers with opposite charges and scalar effective masses, m_1 and m_2, a similar analysis shows that

$$k_\pm^2 \approx -\frac{\varepsilon_L \omega}{c^2}\left[\frac{\omega_{p1}^2}{\omega \pm \omega_{c1}} + \frac{\omega_{p2}^2}{\omega \pm \omega_{c2}}\right] \tag{25}$$

Now the lowest order term in ω/ω_{ci} gives a contribution which is linear in charge and independent of effective mass, and hence vanishes in a compensated plasma ($n_1 = n_2 = n$). Thus, to lowest nonvanishing order:

$$k_+^2 = k_-^2 = \frac{\varepsilon_L \omega^2}{c^2}\left[\frac{\omega_{p1}^2}{\omega_{c1}^2} + \frac{\omega_{p2}^2}{\omega_{c2}^2}\right] = \omega^2 \frac{4\pi n}{B^2}(m_1+m_2) \tag{26}$$

Thus for Alfvén waves, both circular polarizations are propagating and dispersionless, and $\lambda \propto B$.

D. Dimensional Resonances

For a dielectric sphere (indeed a body of any shape) embedded in a material of different dielectric constant, there is a series of electromagnetic "normal mode" oscillations. If the materials were completely lossless, these modes would be self-sustaining: once excited, they would continue to oscillate forever, with no external source. In a real, lossy medium, the oscillations would gradually die out. If the decay time is slow, power may still be easily coupled into the system by coupling to these normal modes. Since these normal modes can generally be considered as "fitting an integral number of wavelengths inside the sphere" (formally, Eq. (3), $ka = \gamma_{ij}$ must be satisfied), there will be a resonant absorption of power as the electromagnetic wavelength is tuned through the value necessary to couple to the mode.

For the problem of a conducting sphere in a magnetic field, Cardona and Rosenblum[16] gave an approximate theory of these dimensional resonances, which explicitly determines the γ_{ij} of Eq. (3) in terms of zeroes of the spherical Bessel functions. Once these γ_{ij} are known, an explicit form for the wave number (eg. Eq. (24) or (26)) can be used to transform the resonance condition, Eq. (3) into an equation for the resonant magnetic field as a function of drop size. The resulting equations are quite different for helicon waves:

$$B = 4\pi nec\omega \left(\frac{a}{c\gamma_{ij}}\right)^2 \qquad (27a)$$

and for Alfvén waves:

$$B = \sqrt{4\pi n(m_1+m_2)} \quad \frac{\omega a}{\gamma_{ij}} \tag{27b}$$

Thus, if power absorption is plotted while the magnetic field is varied, the absorption will appear as a series of resonant peaks, one for each value of γ_{ij}. As the size of the sphere increases, the resonances will shift to higher field, with $B \propto a^2$ for helicon waves, or $B \propto a$ for Alfvén waves.

E. The "Empirical Mie Theory" (EMT)

The theory presented by Cardona and Rosenblum[16,19] (called here the empirical Mie theory (EMT) for scattering by an anisotropic sphere) is based on an assumption which, though plausible, cannot be rigorously justified. Consequently, the validity of any results obtained by this theory can only be tested by comparison to the exact theory. However, by reducing the anisotropic scattering problem to a particular case of Mie theory, analytic results are available. The simple physical picture which these results present can be of great value in attempting to understand the complicated numerical results generated by the exact theory. In Section V, the EMT will be compared to the exact theory,[20] and its usefulness demonstrated.

Mie theory offers an exact solution to the problem of the scattering of a plane electromagnetic wave by a conducting sphere, as long as the conductivity is a scalar, $\overleftrightarrow{\sigma} = \sigma \overleftrightarrow{I}$. In an external magnetic field, even if the conductivity can be written in the diagonal form, Eq. (14),

the diagonal elements are in general not equal. Cardona and Rosenfeld assumed that the absorption due to each diagonal element of the conductivity tensor could be analyzed independently of the other diagonal elements. Furthermore, this absorption was assumed to be the same as that for a sphere having an isotropic conductivity of the same value, either σ_+, σ_-, or σ_3. The anisotropic problem is thereby reduced to Mie scattering for three different isotropic spheres, and the solutions can be found analytically.

The normal modes of Mie theory consist of a series of electric or magnetic multipoles. If the conductivity in the Mie theory is taken as one of the elements of the conductivity tensor appropriate to the helicon problem (single carrier type) the following results are found: (1) There is no resonant absorption in the longitudinal mode (associated with σ_3), and the resonances occur only in one transverse made (σ_- for holes, σ_+ for electrons); (2) in the resonant mode there is an infinite series of resonances, associated with each multipole order. Results are similar for the Alfvén problem, but now there are resonances in both transverse modes. For large fields, these resonances satisfy Eq. (27), with γ_{ij} defined as follows. For each γ_{ij}, 2^i is the multipole order (i=1 for dipole, 2 for quadrupole, etc.), while the j are numbered in order of increasing magnitude of γ_{ij}. For an electric 2^i-pole (magnetic 2^{i+1}-pole) resonance, γ_{ij} is the j^{th} zero of the spherical Bessel function of i^{th} order: $j_i(\gamma_{ij}) = 0$. This quite literally corresponds to fitting j wavelengths inside the sphere.

The problem with this empirical Mie theory is that, once the absorption has been calculated for the three isotropic cases ($\sigma = \sigma_{\pm}$, σ_3), there is no rigorous technique to recombine them to generate the results for the anisotropic case of interest. What has been done in the past is to simply assume that the anisotropic absorption is approximately the sum of the three isotropic cases. This assumption will be analyzed below in Section V.

However, using the analytic solutions from Mie theory, this empirical Mie theory can make some very definite predictions about the properties of these size resonances. For small enough spheres, the resonant field deviates from Eq. (27), and for <u>all</u> modes resonance occurs at the cyclotron field $\omega_c = \omega$ (using Eq. (2) for ω_c). Further, for small spheres, the absorption intensity is predicted to increase as a^{2i+3} for a magnetic 2^i-pole resonance, or as a^{2i+1} for an electric 2^i-pole. The width ΔB of the resonance is proportional to the collision rate, τ^{-1}, and, if τ is independent of magnetic field, ΔB is field-independent for helicon waves, but proportional to B for Alfvén waves.[12] These general features are confirmed by the exact analysis, as will be shown in Section V.

III. EXACT RESULTS FOR DIPOLE ABSORPTION

A. The Solution Inside the Sphere

Following Ford and Werner,[6] the problem is solved by expanding the current in terms of a complete basis set of vector functions over the sphere:

$$\vec{A}^m_\ell(q) = \left(\frac{\ell}{2\ell+1}\right)^{1/2} j_{\ell+1}(qr)\ \vec{Y}^m_{\ell,\ell+1} - \left(\frac{\ell+1}{2\ell+1}\right)^{1/2} j_{\ell-1}(qr)\ \vec{Y}^m_{\ell,\ell-1} \tag{28}$$

$$\vec{B}^m_\ell(q) = \left(\frac{\ell+1}{2\ell+1}\right)^{1/2} j_{\ell+1}(qr)\ \vec{Y}^m_{\ell,\ell+1} + \left(\frac{\ell}{2\ell+1}\right)^{1/2} j_{\ell-1}(qr)\ \vec{Y}^m_{\ell,\ell-1} \tag{29}$$

$$\vec{C}^m_\ell(q) = j_\ell(qr)\ \vec{Y}^m_{\ell,\ell} \tag{30}$$

where the j_ℓ are spherical Bessel functions and the $\vec{Y}^m_{\ell,\ell'}$ are vector spherical harmonics. A summary of the properties of these vector functions is given in Appendix II; the $\vec{A}^m_\ell(q)$ and $\vec{C}^m_\ell(q)$ are constructed so as to be divergenceless, while the $\vec{B}^m_\ell(q)$ are curlless.

Rather then expanding the true current $\vec{j}$ in terms of these functions, we expand the 'pseudo current'

$$\vec{J} = \vec{j} - \frac{i\omega\varepsilon_L}{4\pi}\ \vec{E}\ , \tag{31}$$

By Eq. (5d), this pseudo current is divergenceless, so that the $\vec{B}^m_\ell(q)$ do not appear in its expansion

$$\vec{J}_q = \sum_{\ell,m} a_{\ell m}(q)\ \vec{A}^m_\ell(q) + c_{\ell m}(q)\ \vec{C}^m_\ell(q) \tag{32}$$

If the conductivity tensor $\overleftrightarrow{\sigma}$ has the form (11), Eq. (7) may be rewritten in terms of $\vec{J}$:

$$\vec{\nabla} \times \{\vec{\nabla} \times [\vec{J} + \gamma \hat{z}\hat{z} \cdot \vec{J} + W\hat{z} \times \vec{J}]\} = q_o^2 \vec{J} \tag{33}$$

where γ, W, and q_o^2 are constants defined in terms of the conductivity tensor elements (Appendix III, Eq. AIII.5). Since the $\vec{A}_\ell^m$, $\vec{B}_\ell^m$, and $\vec{C}_\ell^m$ form a complete set of functions, the operations $\vec{\nabla}\times$, $\hat{z}\times$, and $\hat{z}\hat{z}$ applied to these functions can be expressed as linear combinations of these functions (see Appendix II), so that the differential equation (33) is transformed into an algebraic equations linear in the $\vec{A}_\ell^m$ and $\vec{C}_\ell^m$. Since these functions are orthogonal over a sphere, the coefficients of each function must vanish separately. This leads to a system of coupled linear equations, Eq. (AIII.6), in the coefficients $a_{\ell m}$, $c_{\ell m}$, in which q enters as a parameter. This eigenvalue equation has solutions only for particular values of q. For each eigenvalue q, the eigenvectors $a_{\ell m}(q)$, $c_{\ell m}(q)$ define a particular pseudo current $\vec{J}_q$, which is a particular solution of Maxwell's equations inside the sphere. The total current $\vec{J}$ must be a linear combination of these values

$$\vec{J} = \Sigma\, G_q \vec{J}_q \tag{34}$$

where the G_q are determined by boundary conditions at the surface of the sphere.

The matrix equation, presented in Appendix III must be evaluated numerically, but certain simplifying features are evident from its general form. In the first place, the equations do not mix different

values of m. This simplification is made possible by the special form of the conductivity tensor, Eq. (11) - any more general $\overleftrightarrow{\sigma}$ would lead to a mixing of m-values. (This can be seen by analysis of Eq. AII.13). Furthermore, the equations do not mix parity. The functions $\vec{C}^m_\ell$, $\vec{A}^m_{\ell\pm1}$, $\vec{B}^m_{\ell\pm1}$, all have parity $(-1)^\ell$, so that the coefficients can be divided into two series: $\{a_{1m}, c_{2m}, a_{3m},\ldots\}$, and $\{c_{1m}, a_{2m}, c_{3m},\ldots\}$, of which the first series has even parity and the second odd. Only the even series couples to an electric dipole field, whereas the odd series couples only to the magnetic dipole field.

For a given q, the electric field is found to be

$$\vec{E}_q = \frac{4\pi i\omega}{q^2c^2}\,\vec{J}_q + \sum_\ell f'_{\ell m}\,\vec{B}^m_\ell \qquad (35)$$

where the $f'_{\ell m}$ are defined in Eq. AIII.12.

B. Solution Outside the Sphere

Outside of the sphere, the electromagnetic fields also satisfy Eq. (4)-(7), but with $\overleftrightarrow{\sigma} = 0$ and the dielectric constant ε_L appropriate to the medium outside the sphere. Now for a good conductor $\varepsilon_L \ll |\varepsilon|$, where ε is a typical value of $\overleftrightarrow{\varepsilon}$ (Eq. 6), the dielectric constant tensor inside the sphere. Thus there can be a large frequency range ω where $k_0 a \ll 1$ even though $ka \gg 1$, where $k_0 = \sqrt{\varepsilon_L}\,\omega/c$ is the wave vector outside the sphere, and k is the wave vector inside the sphere (e.g.: Eq. (24) or (26)).

In this frequency range, the field equations simplify considerably. The total field can be separated into two parts: an electric part,

Since $\sigma = 0$ outside the sphere, the pseudo current $\vec{J}$ is given by

$$\vec{J} = -\frac{i\omega\epsilon_L}{4\pi}\ \vec{E}\ . \tag{45}$$

C. Boundary Conditions

By standard pill box arguments, it is found that the boundary conditions at the surface of the sphere are continuity of $\vec{B}$, of the tangential component of $\vec{E}$, and of the normal component of $\vec{J}$. Again, by using the orthogonality of the scalar and vector spherical harmonics, these equations become a matrix of linear equations, relating the coefficients G_q, $F^m_{1\ell}$, and $F^m_{2\ell}$ of Eqs. (34)-(35), and (40)-(45). These equations are: for the normal component of $\vec{J}$:

$$\sum_q G_q\ a_{\ell m}(q)\ \frac{j_\ell(qa)}{qa} = -\frac{i\omega\epsilon^o_L}{4\pi\sqrt{\ell}}\left[\frac{F^m_{1\ell}}{\sqrt{2\ell+1}} - D_{Em}\ \delta_{\ell 1}\right]; \tag{46}$$

for the transverse component of $\vec{E}$:

$$\sum_q G_q \left\{\frac{4\pi i\omega}{q^2c^2(2\ell+1)}\ a_{\ell m}(q)\left[\ell j_{\ell+1}(qa) - (\ell+1)j_{\ell-1}(qa)\right] + f'_{\ell m}\ \sqrt{\ell(\ell+1)}\ \frac{j_\ell(qa)}{qa}\right\}$$

$$= F^m_{1\ell}\ \sqrt{\frac{\ell}{2\ell+1}} + 2D_{Em}\ \delta_{\ell 1}\ , \tag{47}$$

where $\delta_{\ell 1}$ is the Krorecker delta function $\delta_{\ell 1} = 1$ if $\ell=1$, $=0$ otherwise; and

$$D_{Em} = \sqrt{\frac{2\pi}{3}}\ \hat{e}^*_m \cdot \vec{E}_1 \tag{48}$$

Further ε_L^o is the dielectric constant outside the sphere, which may differ from ε_L in the sphere. These equations may be rewritten

$$F_{1\ell}^m = \sqrt{3}\, D_{Em}\, \delta_{\ell 1} - \frac{4\pi}{i\omega\, \varepsilon_L^o}\, \sqrt{\ell(2\ell+1)}\, \sum_q G_q\, a_{\ell m}(q)\, \frac{j_\ell(qa)}{qa} \qquad (49)$$

$$\sum_q G_q \left\{ \frac{4\pi i\omega}{q^2 c^2} \left[j_{\ell+1}(qa) - \frac{(\ell+1)\, j_\ell(qa)}{qa} \right] a_{\ell m}(q) + \left[f_{\ell m} - \frac{4\pi i}{\omega \varepsilon_L^o}\, \ell\, a_{\ell m} \right] \frac{j_\ell(qa)}{qa} \right\}$$

$$= 3 D_{Em}\, \delta_{\ell 1} \qquad (50)$$

($f_{\ell m}$ is defined by Eq. AIII.13). Similarly, continuity of the magnetic field results in the equations:

$$F_{2\ell}^m = \frac{-4\pi i}{c}\, \sum_q G_q \sqrt{\frac{\ell}{2\ell+1}}\, j_{\ell+1}(qa)\, \frac{c_{\ell m}}{q} \qquad (51)$$

$$\frac{4\pi i}{c} \sum_q G_q\, \frac{c_{\ell m}}{q}\, j_{\ell-1}(qa) = 3 D_{Bm}\, \delta_{\ell 1} \qquad (52)$$

$$D_{Bm} = \sqrt{\frac{2\pi}{3}}\, \hat{e}_m^* \cdot \vec{B}_1 \qquad (53)$$

The coefficients $a_{\ell m}(q)$ and $c_{\ell m}(q)$ are assumed to be known (Section III.A). Note that D_{Em} couples only to the even parity series (odd $a_{\ell m}$, even $c_{\ell m}$), while D_{Bm} couples to the odd parity series. Thus, in studying the purely electric dipole modes of the sphere ($D_{Bm} = 0$), the odd parity solutions are not excited. The even parity solution is found by solving the matrix equation

$$\overleftrightarrow{R}_E \cdot \vec{G} = 3D_{Em}\, \delta_{\ell 1} \tag{54}$$

where $\overleftrightarrow{R}_E$ is a tensor transforming vectors in q-space into vectors in ℓ-space, which can be explicitly written as:

$$R_{E\ell q} \begin{cases} = \frac{4\pi i\omega}{c^2 q^2} \left[j_{\ell+1}(qa) - \frac{(\ell+1)\, j_\ell(qa)}{qa} \right] a_{\ell m} + \left[f_{\ell m} - \frac{4\pi i}{\omega \varepsilon_L^o}\, \ell a_{\ell m} \right] \frac{j_\ell(qa)}{qa}, & \ell \text{ odd} \quad (55a) \\ = \frac{4\pi i a}{c}\, c_{\ell m}\, \frac{j_{\ell-1}(qa)}{qa}, & \ell \text{ even} \quad (55b) \end{cases}$$

A similar solution can be found for the magnetic dipole case,

$$\overleftrightarrow{R}_B \cdot \vec{G} = 3D_{Bm}\, \delta_{\ell 1} \tag{56}$$

where $\overleftrightarrow{R}_B$ is defined similarly to $\overleftrightarrow{R}_E$, with odd and even rows interchanged.

Once the G_q are found by inversion of Eq. (54) (or 56), the entire current and field distribution inside the sphere can be calculated. However, it is often sufficient to calculate only the total power absorbed by the sphere, which can be found much more easily. The power absorbed is simply $P = \frac{\omega}{2} \mathrm{Im}(\vec{E}_1^* \cdot \vec{P})$ for electric dipole absorption, where the dipole moment $\vec{P}$ is defined by

$$\vec{P} = - \frac{a^3}{(8\pi)^{1/2}} \sum_{-1}^{1} F_{11}^m\, \hat{e}_m \,. \tag{57}$$

Similarly the magnetic dipole absorption is proportional to $\mathrm{Im}(\vec{B}_1^* \cdot \vec{M})$, with

$$\vec{M} = - \frac{a^3}{(8\pi)^{1/2}} \sum_{-1}^{1} F_{21}^{m} \hat{e}_m \tag{58}$$

Thus all that is required is the calculation of the coefficients F_{11}^{m}, F_{21}^{m}. These can be found much more simply, using formal matrix manipulation. Thus, by Cramer's rule,[22] the solution to Eq. (54) is given by

$$G_q = 3D_{Em} \frac{\text{cof}(R_{E1q})}{\det (R_E)} \tag{59}$$

where det(A) is the determinant of the matrix $\overleftrightarrow{A}$, while $\text{cof}(A_{ij})$ is the cofactor of the ijth element of the matrix $\overleftrightarrow{A}$; that is, $\text{cof}(A_{ij})$ is the determinant of the reduced matrix formed from $\overleftrightarrow{A}$ by deleting the ith row and jth column.[22] Using Eq. (59), and the result[22]

$$\det(A) = \sum_j A_{ij} \, \text{cof}(A_{ij}) \quad , \quad \text{for any i,} \tag{60}$$

we may rewrite Eq. (49) as

$$F_{1\ell}^{m} = D_{Em}\left(\sqrt{3}\,\delta_{\ell 1} - \sqrt{\ell(2\ell+1)}\,\frac{12\pi}{i\omega\epsilon_L^o}\,\frac{\det(S_E)}{\det(R_E)}\right), \tag{61}$$

where $S_{E\ell'q} = R_{E\ell'q} \qquad \ell' \neq 1$

$$S_{E1q} = a_{\ell m}\,\frac{j_\ell(qa)}{qa} \tag{62}$$

Similarly,

$$F^{m}_{2\ell} = -3\sqrt{\frac{\ell}{2\ell+1}}\quad D_{Bm}\,\frac{\det(S_B)}{\det(R_B)} \tag{63}$$

$$S_{B1q} = j_{\ell+1}(qa)\ c_{\ell m}/qa \tag{64}$$

Formally, the matrices $\overleftrightarrow{R}$ and $\overleftrightarrow{S}$ are infinite dimentional, involving an infinite number of $a_{\ell m}$'s and $c_{\ell m}$'s. In practice the equations are truncated at some ℓ_{max}, and solved numerically on a CDC 7600 computer. It is found that the resulting power absorption converges to a fixed value as ℓ_{max} increases and that larger values of ℓ_{max} are required as the sphere radius a increases. Results of these numerical calculations will be presented in Section V.

In the calculations presented here, values of ℓ_{max} up to 24 have been used. Beyond this point, the numerical accuracy of the calculations (single precision was used) becomes insufficient to produce meaningful results.

The above solutions have all been dipole modes of the sphere - that is they are excited by spatially uniform electric and magnetic fields. If the sphere is large enough, the condition $k_o a \ll 1$ is no longer well satisfied (k_o is the wave number outside the sphere - see Section B). In this case it should be possible to observe higher multipole resonances of the sphere. The calculations of this section can be extended to describe these. Ref. 6 has an example of the calculation of magnetic quadrupole resonances, and Ref. 22 presents a formal solution to the full Mie theory for an anisotropic sphere - including all multipole modes.

IV. THE APPROXIMATE SOLUTION

In Ref. 18, Ford, Furdyna and Werner presented an alternative, but approximate, solution to the problem of helicon waves in a sphere. This solution is much easier to handle than the exact solution and can readily be used to analyze experimental data. While this solution is incomplete and does not show as rich a spectrum of resonances as the exact solution, it has the advantage that it may be generalized for a sphere with an arbitrary conductivity tensor, as will now be shown. Hence it provides new information not readily available from the exact solution. As an illustration, in Section V the angle dependence of the principal Alfvén resonances will be derived for EHD in both strained and unstrained Ge.

The approximation scheme involves a perturbation expansion of the internal fields in powers of the radius of the sphere. Hence the resulting absorption agrees with the exact calculation in the small sphere limit. The perturbation expansion is explicitly carried out to second order, and from this result an empirical expression is formed which agrees with the perturbation result to second-order, but gives improved agreement with the exact result (in the cases in which this result is known). Following Ref. 18, the pseudocurrent $\vec{J}$ (Eq. 31) is expanded

$$\vec{J} = \vec{J}^{(0)} + \vec{J}^{(1)} + \ldots . \tag{65}$$

where $\vec{J}^{(n)} \propto a^{2n}$; similar expansions are formed for $\vec{B}$ and $\vec{E}$. Inside the sphere, these fields and currents are found by solving Maxwell's equations (Eq. 4 and 5) sequentially:

$$\vec{J}^{(n)} = \overleftrightarrow{\sigma} \cdot \vec{E}^{(n)} \tag{66}$$

$$\vec{\nabla} \times \vec{B}^{(n)} = \frac{4\pi}{c} \vec{J}^{(n)} \tag{67}$$

$$\vec{\nabla} \times \vec{E}^{(n+1)} = \frac{i\omega}{c} \vec{B}^{(n)} \tag{68}$$

These equations may be solved with an arbitrary conductivity tensor $\overleftrightarrow{\sigma}$. For electric dipole modes $\vec{E}^{(0)} = \vec{E}_1$ (Eq. 43), $\vec{B}^{(0)} = 0$; for magnetic modes $\vec{E}^{(0)} = 0$, $\vec{B}^{(0)} = \vec{B}_1$. Outside the sphere, the solutions are simplified: for the electric dipole modes the magnetic field is neglected, while the electric field is given by Eq. (36); the boundary conditions which are satisfied are the continuity of the tangential component of $\vec{E}$ and of the normal component of $\vec{J}$. Conversely, for magnetic dipole fields, the external electric field is ignored, while the magnetic field satisfies Eq. (38) outside the sphere, and is continuous across the surface. Again, the primary quantity of interest is the power absorbed, which can be written in terms of the dipole moment of the sphere, as in Eqs. (57) (electric dipole). To order $\vec{E}^{(1)}$, the electric dipole moment can be written

$$\vec{P} = -\frac{a^3}{\sqrt{8\pi}} \sum_{m=-1}^{1} f_{11}^m \hat{e}_m \tag{69}$$

where

$$f_{11}^m = \sqrt{2\pi} \left[\delta_{mn} - 3\mathcal{D}_{mn}^E \right] \hat{e}_n^* \cdot \vec{E}_1 \tag{70}$$

$$\mathcal{D}_{mn}^E = B_{mn}^{-1} + B_{mn'}^{-1} \frac{\omega^2 a^2 \varepsilon_L}{5c^2} B_{n'n}^{-1} \tag{71a}$$

$$\simeq \left(B_{mn} - \frac{\omega^2 a^2 \varepsilon_L}{5c^2} \delta_{mn} \right)^{-1} \tag{71b}$$

and

$$B_{mn} = \delta_{mn} - \frac{i\omega\varepsilon_L}{2\pi}\rho_{mn} \tag{72}$$

$\overleftrightarrow{p} = \overleftrightarrow{\sigma}$ being the resistivity tensor. Equation (71a) is the direct second order perturbation result. Equation (71b) is adapted following Ref. 18: when expanded in powers of a^2, it agrees with the earlier result, and is chosen to give better agreement with the exact result for larger spheres. In an analogous fashion the magnetic dipole moment can be written (Eq. (58))

$$\vec{M} = -\frac{a^3}{\sqrt{8\pi}}\sum_{m=-1}^{1} f_{21}^{m}\,\hat{e}_m \tag{73}$$

$$f_{21}^{m} = -\frac{\sqrt{2\pi}\,i}{15}\,\frac{4\pi\omega^2 a^2}{c^2}\,\mathcal{D}_{mn}^{M}\,\hat{e}_n^{*}\cdot\vec{B}_1 \tag{74}$$

$$\mathcal{D}_{mn}^{M} = D_{mn}^{-1} + D_{mn'}^{-1}\,\frac{8\pi i\omega^2 a^2}{21c^2}\,D_{n'n}^{-1} \tag{75a}$$

$$\simeq \left(D_{mn} - \frac{8\pi i\omega^2 a^2}{21c^2}\,\delta_{mn}\right)^{-1} \tag{75b}$$

$$D_{mn} = \omega\bar{\rho}_{mn} \equiv \omega(\delta_{mn}\,\mathrm{Tr}(\overleftrightarrow{\rho}) - \rho_{nm}) \tag{76}$$

(This form of D_{mn} was first presented in Ref. 24.)

The above results are applied to electron-hole drops in Ge in the following section, and the results are compared to the exact results of Section III.

V. APPLICATION: DIMENSIONAL RESONANCES IN ELECTRON-HOLE DROPS IN Ge

A. Introduction

Dimensional resonances, of the form discussed in Section II.E, have been observed in the absorption of microwave power due to large electron-hole drops (γ-drops) formed in nonuniformly stressed Ge.[7,8] In fact, the existence of these large drops was first inferred from these resonances, and their size estimated from the simplified theory of Section II.E. The results of the previous sections can be used to obtain a more rigorous description of these resonances.

Due to the multi-valley conduction band in Ge, the conductivity tensor inside an EHD can be written in the form of Eq. (9), only if the magnetic field is aligned along a high-symmetry axis of the crystal. In unstrained Ge, when all four conduction band valleys are equally populated (Ge(4:2)), these high symmetry directions are along ⟨100⟩ and ⟨111⟩ axes. However, the large γ-drops have only been produced in the presence of a large ⟨111⟩-stress.[14] This stress lowers one valley with respect to the other three, with the result that inside the γ-drop only one valley is populated by carriers, to any significant extent. In this case the symmetry is reduced, and the exact solution can be found only if the field lies along the stress axis. The case in which the field lies along other directions can be treated approximately, as discussed in the previous section.

The valence band in Ge is doubly degenerate at zero stress ("heavy" and "light" holes). This degeneracy causes the hole bands to be warped and greatly complicates the analysis of the hole conductivity, particularly

in a magnetic field. The stress acts to split these two bands, and at high stresses all of the holes are in a single ellipsoidal band. The stress required to depopulate one hole band is considerably larger than that needed to depopulate the three conduction band valleys, and in the experimentally observed γ-drops the holes are thought to lie somewhat closer to the zero-stress limit. The complications of the valence band are for the most part ignored in this paper. In zero stress the holes are treated as two decoupled spherical bands.[25] Two limiting cases will be analyzed: [1] Ge(1:2), in which only one conduction is occupied, but the holes are treated in the unstressed limit; and [2] Ge(1:1), in which only a single, ellipsoidal hole band is occupied.

In summary, the exact theory can be solved in four situations: $B\|\langle 100\rangle$: Ge(4:2) and $B\|\langle 111\rangle$: Ge(4:2), Ge(1:2), and Ge(1:1). The conductivity tensors in these four cases are derived in Appendix I. The resulting spectra are qualitatively similar in all four cases, and only Ge(1:2) will be analyzed in detail. This is the case which most closely corresponds to the observed γ-drops.

B. Size-Dependent Resonances: Magnetic Dipole

Figure 2(a-c) shows typical magnetic dipole absorption spectra, plotting microwave absorption as a function of magnetic field for a variety of drop sizes. The three sets of spectra correspond to the three possible polarizations of the microwave magnetic field, $\vec{B}_1$, with respect to the static field, $\vec{B}$. The LM resonances (longitudinal magnetic, with $\vec{B}_1 \| \vec{B}$) are shown in Fig. 2a, while the circularly polarized TM ± (transverse - $\vec{B}_1 \perp \vec{B}$)

are in Figs. 2b and 2c. The signs ± are defined through Eq. (44): for TM+, $\vec{B}_1 \parallel \hat{e}_{+1}$. For helicon waves, with only one species of carrier, one direction of circular polarization is inactive. For example, if there are only electrons (negatively-charged carriers), the size-dependent resonances occur only for the TM+ and LM polarizations. In EHD, because there is an equal number of electrons and holes, both transverse modes are resonance-active. However, there is still a sense in which the TM- resonances are associated with holes and the TM+ resonances with electrons. This will be discussed further in subsection C, when the Rayleigh limit is considered, and in Section VI, when, by varying the material parameters, the transition from Alfvén to helicon waves is studied.

For all of the theoretical curves in this section, the following material parameters were used: lattice dielectric $\varepsilon_L = 15.38$, microwave frequency, $\omega/2\pi = 25$ GHz, and collision frequency $\tau_e = \tau_h \equiv \tau = 100/\omega$. The last is chosen to give sharp resonances. The pair density inside the EHL decreases greatly with stress, and the following values are used: for Ge(4:2), $n = 2.3 \times 10^{17}$ cm^{-3} [9,26]; for Ge(1:2), $n = 0.5 \times 10^{17}$ cm^{-3} [15]; for Ge(1:1), $n = 0.11 \times 10^{17}$ cm^{-3}.[26]

The theoretical spectra were calculated as in Fig. 2, varying field for fixed drop radius. Generally, the field was sampled in 100 G increments, and radii taken in 10 μm intervals (25 μm for Ge(1:1)). For small drops, and to sort out complicated structure, smaller size intervals were used; while in order to study line shape and peak height, fields near the resonances were studied in 10 G intervals. The convergence of the numerical technique was checked throughout the range studied. However, outside this range (larger drops and higher fields), the

numerical convergence gradually becomes unsatisfactory.

The spectra of Fig. 2 show a great profusion of resonances. In Fig. 3 the peak positions of these resonances are plotted as a function of drop size in the three different modes. Only the more intense, higher field modes (labeled in the figures) have been studied in detail. At lower fields some relatively prominent peaks have also been indicated in the figures, but there are many still weaker resonances which have been omitted for clarity.

This large number of resonances is in marked contrast to the result of the empirical Mie theory (EMT) (Section II.E). For each (transverse)[27] magnetic dipole, the EMT predicts a single series of resonances, occurring at fields

$$B_m = \sqrt{\frac{nM}{\pi}}\ \frac{\omega a}{\gamma_{1m}} \tag{77}$$

where $M = m_e + m_h$, and $\gamma_{1m} = m\pi$, with m an integer > 0. The origin of the additional resonances in the exact theory can be readily understood. In the Mie theory for isotropic spheres, the different multipole excitations of the sphere are orthogonal, much as the normal modes of a rectangular microwave resonant cavity. The static magnetic field, which introduces an anisotropy into the conductivity tensor, breaks the spherical symmetry and acts much as a nonsymmetric perturbation in a cavity. Such a perturbation has two major consequences. First, the original modes are no longer orthogonal. Consequently, a field which was originally (in the absence of the perturbation) purely dipole, will now couple weakly to resonances associated with all multipoles, hence greatly increasing the number of "dipole" resonances observed. Secondly, resonances associated with

different multipole orders are no longer orthogonal. If, in the unperturbed system, two resonances of different order would have crossed each other (as drop size varied), in the perturbed system these resonances are not orthogonal, and can no longer cross. Instead, complicated anti-crossing phenomena are observed, where the properties of the two resonances are gradually interchanged while the two resonances never get closer in field than a certain minimum distance.

Such anti-crossing behavior is readily apparent in the curves of Fig. 3. Indeed, in each figure all of the labeled curves (a-d) correspond to the single γ_{11}-resonance of EMT, crossing a series of much weaker resonances. That this is indeed the case should be clear from Fig. 4, which plots the intensities of the labeled modes as a function of drop size. Clearly the intensity is successively being transferred from a to b to c to d as the drop radius increases. Such behavior is absent both in the EMT and in the approximate analytic theory of Section IV. The results of the approximate theory are presented as dashed lines in Figs. 3 and 4. It can be seen that this theory gives a good account of the average behavior of the resonances (intensity and resonant field), but does not show all the complexity introduced by the multiple resonances and anti-crossing behavior.

The approximate theory, by its construction, describes only the lowest order dipole resonance. The higher order dipole resonances of the EMT (Eq. (77) with $m > 1$) do show up in the exact theory as the weaker resonances observed at lower fields (the unlabeled lines in Fig. 3). Only for the LM modes is the anti-crossing behavior[28] weak enough to test the predicted EMT values for successive γ_{1m}: the dots in Fig. 3a

correspond to straight lines through the origin[29] with slopes in the ratio 1:1/2:1/3, and it is seen that the results of the exact calculation approximately agree with this.

Note in Fig. 4 that for small drops ($a < 50$ μm), the absorption intensity increases as a^5, in accord with the prediction of the EMT, but for larger drops the absorption saturates, increasing approximately as a^3 in the largest drops.[30] In these figures, what is actually plotted is χ'', the imaginary part of the magnetic susceptibility, where $\vec{M} \equiv \chi V \vec{B}$, and V is the drop volume. The absorbed power P is equal to $\omega/2 \, \mathrm{Im}(\vec{M} \cdot \vec{B})$, or

$$P = \frac{\omega}{2} |B|^2 V\chi'' \tag{78}$$

Note that although χ'' saturates in large drops, the integrated power per unit volume continues to increase since the linewidth increases with field.

Figure 5 plots the linewidth (full width at half maximum) of the principal resonances as a function of field, comparing the exact (solid line) and approximate (dashed line) theories. The approximate theory is seen to slightly overestimate the linewidth. As predicted by the EMT, the linewidth increases approximately linearly with B. Note for the LM mode that above the c-d line-crossing there is evidence of further, weaker anti-crossing phenomena. Even though the weaker peak cannot easily be detected directly (it occurs more as a shoulder than a separate peak, for $\omega\tau = 100$), these phenomena can still lead to oscillatory structure in the peak intensity and linewidth.

Figure 6 plots the analogous peak position vs. field for the other exactly soluble cases: Ge(4:2), $B \| \langle 100 \rangle$ (Fig. 6a); Ge(4:2), $B \| \langle 111 \rangle$ (Fig. 6b); and Ge(1:1), $B \| \langle 111 \rangle$ (Fig. 6c). The principal difference

(note scale changes) is due to the very different pair densities in these cases: as in Eq. (77), $B \propto n^{\frac{1}{2}}a$. In fact, all the spectra appear quite similar if plotted[12] as B vs. $\alpha(Mn)^{\frac{1}{2}}a$. Here $M = m_e + m_h$,[31] and α is a "fudge factor," which empirically measures the difference between the exact theory and the EMT (for which α would be equal to one). If $\alpha(Ge(1:2)) \equiv 1$, then $\alpha = 1.02$ (Ge(4:2), $B \| \langle 100 \rangle$), 1.13 (Ge(4:2), $B \| \langle 111 \rangle$), 1.12 (Ge(1:1)). The intensities, linewidths, and anti-crossing behavior are similar in all these cases.

C. The Rayleigh Limit

In the EMT it is found that as the drop radius becomes very small (smaller than the wavelength inside the drop), the resonances all shift to the cyclotron resonance field, and the field position becomes independent of a. While the resonances in Fig. 3 do have radius-independent limiting fields in this Rayleigh limit, the fields are not equal to the cyclotron fields and in fact are not the same for all resonances.

Indeed, if all the resonances had the same Rayleigh limit, most of the anti-crossing behavior would be eliminated: if all of the resonances were straight lines (when plotted as B vs. a) coming from the same origin, they would simply fan out and never cross.[33] What is happening in Fig. 3 is that the curves with smaller slopes (curves b,c,d) start out from a higher Rayleigh limit field. Consequently, the a-curve, with larger slope, gradually "catches up" with them and the anti-crossings result.

A simple physical model can explain both the correct Rayleigh limit of the dipole mode as well as the higher Rayleigh limits associated with the higher-order multipole resonances. Figure 1 shows the field distri-

bution inside a sphere near the lowest transverse dipole resonances. The figure is schematic in that the fields were calculated in the Mie theory for an isotropic sphere, but should be approximately correct, particularly in the Rayleigh limit. The induced current approximately follows $\vec{E}$, and circulates in loops about the microwave magnetic field. Consequently, for the transverse modes, the current flows half of the time along the external field, and half perpendicular to it. Since resistances add in series the effective conductivity is $\sigma_{\pm}^{eff} = \frac{1}{2}(\sigma_{\pm}^{-1} + \sigma_3^{-1})^{-1}$. For a simple scalar mass carrier of mass m, $\sigma_3^{-1} \propto m$, $\sigma_{\pm}^{-1} \propto m(1 \pm \omega_c/\omega)$,[34] so that

$$(\sigma_{\pm}^{eff})^{-1} \propto m\left(1 \pm \frac{\omega_c}{2\omega}\right) \tag{79}$$

The resonance condition, $\sigma_{\pm}^{eff} \to \infty$, becomes $\omega_c = \pm 2\omega$ — that is, the resonance occurs at twice the cyclotron resonance field. That this is indeed approximately the case is shown by arrows in Figs. 3b and 3c. Note that for the TM- mode, the mass associated with the resonance is the hole mass ($eB/\omega c = 2m_h$), while for the TM+ mode it is the electron mass. Similar reasoning applied to the LM mode would suggest $\sigma^{eff} = (\sigma_+^{-1} + \sigma_-^{-1})^{-1}$, or a resonance at a field $eB/\omega c = 2m_r$, where $m_r^{-1} = m_e^{-1} + m_h^{-1}$. The arrow in Fig. 3a shows this to be the case.

The Rayleigh limit of these resonances is analyzed further in Section V.D, in which the angle dependence of the resonances is studied (Fig. 9a) and in Section VI, in which the resonances are studied as m_h is varied. It is seen there that the considerations of the present section are valid only near the Alfvén limit — that is, when m_e and m_h have comparable magnitudes. If $m_h >> m_e$, the TM- resonance occurs near the hole cyclotron

resonance field, and not at twice that value.

For higher multipole configurations, the fields presumably are similar to those shown in Fig. 7. These were constructed as in Fig. 1, using the results of the Mie theory. By an argument similar to that given above, for a 2^i-pole resonance, the carrier moves perpendicular to $\vec{B}_o$ for only a fraction 1/2i of its orbit. Consequently, the effective conductivity is $(\sigma_\pm^{eff})^{-1} \sim m(1 \pm \omega_c/2i\omega)$, and the resonance occurs at a field

$$\omega_c = \pm 2i\omega \tag{80}$$

Because of the complications of the Ge band structure, the resonant fields will be slightly modified, but inspection of Fig. 3 shows that the above resonance conditions are approximately valid. Since the TM+ and TM- resonances appear to have the same zero-field limit, the arrows depict the average field found from Eq. (80) for electrons and holes.

D. Angle Dependence of the Resonances

The approximate theory can be used to study the angle dependence of these resonances. Figure 8 shows the angle dependence in a (110)-plane of the resonances for a 40 μm radius drop for the three cases Ge(1:2) (Fig. 8a); Ge(4:2) (Fig. 8b), and Ge(1:1) (Fig. 8c). Because there are four populated electron valleys in Ge(4:2), the spectra have 90° symmetry, while in the other cases there is only 180° symmetry. In Fig. 8, the exact resonances are also plotted along those symmetry directions for which the theory of Section III can be applied. The agreement is quite good for Ge(1:2) and Ge(1:1), but less so for Ge(4:2), where, due to the

higher pair density, mode anti-crossing phenomena are already important. Away from the symmetry directions, the peaks are no longer purely longitudinal or transverse: there are generally absorption peaks in all three modes, only slightly shifted from one another in field, although differing greatly in intensity. For the most part, the lowest lying mode is predominantly LM, with the most intense absorption in this branch (along the symmetry directions it is purely LM). The highest field mode is predominantly TM-, and the intermediate mode TM+.

The complex angle dependence can approximately be understood from the simple considerations of the EMT and Section V.C. The solid lines in Fig. 9a show the Rayleigh limit resonances for Ge(1:2) ($a = 1$ μm). Along with them are plotted the results expected from the previous section: the dashed lines represent cyclotron resonance fields for carriers with effective masses $2m_e$ (curve 1), $2m_h$ (curve 2), and $2m_r$ (curve 3). While there is much evidence of interaction between the different resonances, the three dashed curves give a qualitative picture of the real angle dependence. As expected, the TM- mode is similar to m_h, the TM+ to m_e, and the LM to m_r.

At higher fields, the EMT predicts an angle dependence $\propto \sqrt{M} = \sqrt{m_e + m_h}$. This angle dependence is plotted in Fig. 9b, along with the angle dependence found from the approximate theory of Section IV, for a drop with 120 μm radius. While the "LM" resonance has an angle dependence similar to $\sqrt{M}$, the "TM-" mode has a much stronger variation with angle - it is quite similar to the cyclotron resonance of the electrons (curve 1 of Fig. 9a).

E. Size-Dependent Resonances: Electric Dipole

The electric dipole modes form an interesting comparison. While the EMT predicts a series of electric dipole size-resonances, increasing in intensity as a^3, a simple physical argument suggests that this is not the case. The electric dipole fields should look approximately like Fig. 1, with $\vec{E}$ and $\vec{B}$ interchanged. In this case the electric field, and consequently the current, will have components perpendicular to the drop surface. These fields will induce surface charge and correspondingly large depolarization fields. This in turn will cause any resonances to be shifted to high frequencies or high fields — the usual plasma resonance and plasma-shifted cyclotron resonance.[3] However, this argument holds only if the induced field is spatially uniform, and begins to break down if there are several wavelengths inside the sphere.

These arguments are confirmed by the results of the exact calculation. These results are displaced in Figs. 10-14, which correspond to Figs. 2-6 for the magnetic modes. There are no size-dependent resonances which increase in intensity as a^3 or a^5. Even for the largest drops, the resonances are weak compared to the magnetic dipole resonances and fall off faster with drop size as a decreases (like a^7, or even faster). Indeed, in the approximate theory of Section IV, these resonances do not appear at all.

There is, however, a rich spectrum of these weak resonances. The LE resonances appear similar to the TM resonances, while the TE resonances are quite complicated, and occur at generally lower magnetic fields. These resonances may be observable experimentally, since they are generally

separated in field from the more intense magnetic resonances.

In addition to these size-dependent resonances, there are several other electric dipole resonances, which have intensities $\propto a^3$. While the resonant field does change weakly with a, this is a small effect, and the origin of these resonances can be understood from a simple Rayleigh-limit theory[3,35] of plasma-shifted cyclotron resonance. The net field inside the sphere is the sum of the external field plus a depolarization field

$$\vec{E}_{eff} = \vec{E} - \overleftrightarrow{L} \cdot \vec{P} \tag{81}$$

$$\vec{P} = \chi_o \vec{E}_{eff} + n e \vec{r} \tag{82}$$

where $\overleftrightarrow{L}$ is a depolarization tensor ($\overleftrightarrow{L} = 4\pi/3\ \overleftrightarrow{I}$ for a sphere), and χ_o is the background susceptibility in the drop: $\varepsilon_L = 1 + 4\pi\chi_o$. If $\vec{E}_{eff}$ is used in Eq. (8), the resistivity tensor becomes

$$\overleftrightarrow{\rho}_{eff} = \frac{\overleftrightarrow{\rho} + i(\overleftrightarrow{I} + \chi\overleftrightarrow{L})^{-1} \cdot \overleftrightarrow{L}}{\omega} \equiv (\overleftrightarrow{\sigma}_{eff})^{-1} \tag{83}$$

while the absorbed power is $\vec{P} = \frac{1}{2}\vec{E} \cdot \overleftrightarrow{\sigma}_{eff} \cdot \vec{E}$. If $\overleftrightarrow{\sigma}$ is written in the form AI.1 (as in Appendix I), this amounts to replacing M_1 and M_3 by $M_i^{eff} = M_i - \bar{\omega}_p^2/\omega^2$, where $\bar{\omega}_p^2 = \frac{L}{1+\chi_o L} ne^2$. For a single scalar mass particle $M_3 = m$, and the longitudinal resonance condition is $\omega^2 = \bar{\omega}_p^2/m \equiv \hat{\omega}_p^2$. For the transverse case $M_1 \simeq m(1 - \omega_c^2/\omega^2)$, while $M_2 \simeq -\frac{\omega}{\omega_c} m(1 - \omega_c^2/\omega^2)$. Diagonalizing $\overleftrightarrow{\sigma}_{eff}$, the resonance condition is found to be $M_1^{-1} \pm M_2^{-1} = (\bar{\omega}_p/\omega)^{-2}$, or

$$1 \pm \frac{\omega_c}{\omega} = \left(\frac{\hat{\omega}_p}{\omega}\right)^2 \tag{84}$$

This is the plasma-shifted cyclotron resonance. For $\hat{\omega}_p \to 0$, the ordinary cyclotron resonance $\omega = \mp\omega_c$ is recovered. If $\hat{\omega}_p >> \omega$, only the plasma-shifted resonance $\omega_c = \pm\hat{\omega}_p^2/\omega$ is observed.

If there are several types of carriers, it is possible that not all the resonance lines will be shifted to the plasma frequency. Thus when there are two holes, only one resonance is plasma-shifted to high fields while the other, although shifted from its low-density cyclotron field, remains at a low field.[35] Similarly, in Ge(4:2), the presence of several ellipsoidal conduction band minima leads to a number of resonances which are not plasma shifted. For EHD in Ge, these resonances can be found by using the appropriate $\overleftrightarrow{\sigma}$ in the above theory; they are discussed in Refs. 12,31,36. For Ge(4:2), the angle dependence of these resonances is shown in Fig. 15 (calculated from the approximate theory of Section IV). All of the resonances are due to the multiple electron valleys, except the one at 400 G, which is due to the two hole bands. In Ge(1:2), this is the only resonance which appears. For Ge(1:1), there is only one electron valley and one hole band populated, and consequently none of these "dielectric anomaly" resonances are observed. For an arbitrary angle, these resonances generally occur simultaneously in all three modes, L, $T^{\pm}$, and for magnetic as well as electric dipole absorption. Indeed the magnetic absorption is generally more intense than the electric.

In Figs. 10b and 10c, the low-field tail of the plasma-shifted cyclotron resonance can be observed for small a. These resonances will be discussed in greater detail in a separate paper.

VI. THE TRANSITION FROM ALFVÉN TO HELICON WAVES

Helicon and Alfvén waves are two limiting extremes of the kinds of waves which can be expected in a material with two types of carriers. In Alfvén waves, both types of carriers have a comparable mobility, and the number of carriers of each type are equal. If the conductivity of one species decreases relative to the other, the propagating electromagnetic waves of the system gradually change from Alfvén-like to helicon-like behavior. The present theory of electromagnetic absorption by a sphere offers a convenient means of studying this transition.

For simplicity, the material parameters will be chosen similar to the EHD in Ge, except that the carriers will be assumed to have scalar masses: the initial, Alfvén-state, is taken to have $m_e = 0.12\ m_o$, $m_h = 0.30\ m_o$, $n_e = n_h = 5 \times 10^{16}\ cm^{-3}$, $\omega\tau_e = \omega\tau_h = 100$. The dimensional resonances of the system are analyzed using the approximate theory of Section IV.

The transition to the helicon-state can occur in any of three essentially different ways. Either the mass of one particle can become very large, or its concentration quite small, or its scattering time very short. All three of these cases lead to the same final state. If the holes are eliminated, then the final state has dimensional resonances only in the TM+ case. These resonances are typically helicon-like: the resonant field increases as a^2, and the linewidth of the resonance is independent of magnetic field.

The manner in which the TM- and LM resonances disappear varies greatly in the three cases. In each case, however, both resonances

change qualitatively in the same manner, with the TM- resonance disappearing sooner.

Figure 16 shows how the resonances change as the hole mass is increased. The resonant field is plotted vs. hole mass in Fig. 17a, for a drop with a = 1 μm (the Rayleigh limit spectrum). For large enough m_h, the TM- resonance occurs slightly above the hole cyclotron resonance field (not at twice this field, as suggested by the discussion of Section V.C), and the resonant field shifts linearly with m_h. The LM resonance shifts approximately like $m_h^{\frac{1}{2}}$ — again quite a different result from the considerations of Section V.C — so that, for large enough m_h, it is also shifted to unobservably high fields. A typical intermediate situation is shown in Figs. 17b and 17c ($m_h = 20\ m_e$). For low fields, the TM+ resonance is helicon-like, shifting field as a^2 (the dashed line in Fig. 17b is the helicon limit: $m_h \to \infty$), while the linewidth (Fig. 17c) is independent of field. Once the resonant field approaches the hole cyclotron-resonance field, however, Alfvén-like behavior is observed: $B \propto a$; $\Delta B \propto B$.

If instead, the hole density n_h is reduced, while m_h is constant, quite different resonances are observed. Again the TM+ resonance gradually shifts to the helicon limit, but now the TM- and LM resonances decrease greatly in intensity and gradually become size-independent resonances occurring at the cyclotron field. Figure 17 illustrates an intermediate state $n_h = \frac{1}{2} n_e$.

Finally, if τ_h decreases, the resonances greatly broaden out, and the TM- and LM resonances are lost as their peak intensity goes to zero. The resonances also shift to higher fields, but for $\omega\tau_h \gg 1$, this effect

is small. The TM- resonance essentially vanishes as soon as $\omega\tau_h < 1$, but a weak, broad LM resonance can still be observed for $\omega\tau_h = 0.1$. At first, the TM+ resonance linewidth increases, as illustrated in Fig. 18, but the linewidth starts to decrease again as soon as $\omega\tau_h < 1$, and for small enough τ_h, the linewidth depends only on τ_e. For $\omega\tau_h \leq 0.1$, the TM+ resonant field shifts approximately like a^2, but only for $\omega\tau_h \leq 10^{-3}$ is the linewidth approximately field-independent.

ACKNOWLEDGMENTS

I would like to thank C. D. Jeffries, J. P. Wolfe, G. W. Ford, S. A. Werner, C. Kittel, J. E. Furneaux, L. M. Falicov, J. R. Dixon, Jr., and J. K. Furdyna for interesting and useful discussions, and I would like to thank Drs. Ford and Werner for allowing me to see their calculations prior to publication. This work was supported in part by the U.S. Energy Research and Development Administration. I would also like to thank the General Electric Company for support during the writing of this paper.

APPENDIX I: EFFECTIVE MASSES AND CONDUCTIVITY TENSOR IN Ge

A. Conduction Band

The conduction band in Ge has four equivalent minima, located at the L-point of the Brillouin zone (intersection of ⟨111⟩-direction with zone boundary).[12,14] In each minimum ("valley"), the carrier mass is anisotropic, having one value along its respective ⟨111⟩-axis, $m_\ell = 1.58\ m_o$, and a much lower value perpendicular to that axis, $m_t = 0.082\ m_o$, where m_o is the free electron mass. For a magnetic field along any crystalline direction, the conductivity tensor of electrons in any one valley can be found from Eq. (10). In an EHD in unstrained Ge, all four valleys are equally populated, and the net conductivity tensor is the sum of the four tensors associated with the individual valleys. This procedure is carried out in detail, e.g., in Refs. 35 and 37. If the magnetic field is along an arbitrary crystalline direction, all nine components of the conductivity tensor will, in general, be different from zero, and the exact results found in Section III do not apply. However, if the field is along an axis of at least 3-fold symmetry, the conductivity tensor will have no components linking longitudinal and transverse directions. In this case $\overleftrightarrow{\sigma}$ can be written in the form of Eq. (11), and the calculations of Section III follow. For an EHD in Ge, the three- and four-fold crystal axes lie along ⟨111⟩- and ⟨100⟩-directions. The σ_i of Eq. (11) can explicitly be written as

$$\sigma_i = \frac{\bar{\sigma}_o}{1 - i\omega\tau_e} M_i^{-1} \qquad \text{(AI.1)}$$

where $\bar{\sigma}_o = Ne^2\tau$, and for H∥⟨100⟩:

$$M_1^{-1} = \frac{m_1 m_t}{m_t^2 m_\ell + m_2 \mu_e^2} \tag{AI.2a}$$

$$M_2^{-1} = \frac{-m_2 \mu_e}{m_t^2 m_\ell + m_2 \mu_e^2} \tag{AI.2b}$$

$$M_3^{-1} = \frac{m_1 m_t + \mu_e^2}{m_t^2 m_\ell + m_2 \mu_e^2} \tag{AI.2c}$$

Here $3m_1 = m_t + 2m_\ell$, $3m_2 = 2m_t + m_\ell$, $\mu_e = -|\omega_{co}|\tau_e/[1 - i\omega\tau_e]$, and $\omega_{co} = eB/c$. For $H \| \langle 111 \rangle$

$$M_1^{-1} = \frac{m_t m_\ell}{D}\left(m_t^2 m_1 + \mu_e^2\left(\frac{2m_2 + m_1}{3}\right)\right) \tag{AI.3a}$$

$$M_2^{-1} = -\frac{\mu m_\ell}{D}\left(m_t^2 m_2 + \mu_e^2\left(\frac{2m_t + m_2}{3}\right)\right) \tag{AI.3b}$$

$$M_3^{-1} = \frac{(m_t^2 + \mu_e^2)}{D}\left(m_t m_\ell m_1 + \mu_e^2\left(\frac{2m_\ell + m_2}{3}\right)\right) \tag{AI.3c}$$

and

$$D = m_\ell(m_t^2 + \mu_e^2)\left(m_t^2 m_\ell + \mu_e^2\left(\frac{2m_t + m_2}{3}\right)\right) \tag{AI.4}$$

Under a large uniaxial stress along a ⟨111⟩-direction, the electron ellipsoids are split in energy, with the ellipsoid associated with the strain direction being lowered in energy with respect to the other ellipsoids. It has been possible to produce large masses of EHL in strained Ge, for which only this one valley is occupied,[12,14,15] and size-dependent Alfvén resonances have been observed in the microwave absorption spectrum.[7,8] For this situation the conductivity tensor reduces

to that of a single valley. It can be written in the simpler form of Eq. (11), only if the field is parallel to the stress axis. In this case, $B \| \langle 111 \rangle$, Ge(1:2) or Ge(1:1),

$$M_1^{-1} = \frac{m_t}{m_t^2 + \mu_e^2} \tag{AI.5a}$$

$$M_2^{-1} = -\frac{\mu}{m_t^2 + \mu_e^2} \tag{AI.5b}$$

$$M_3^{-1} = m_\ell^{-1} \tag{AI.5c}$$

Note that here m_t and m_ℓ are completely decoupled, and M_3^{-1} is independent of the magnetic field. In the previous cases M_3 goes to a constant as B becomes infinite, but there is a longitudinal magnetoresistance (i.e. M_3 is field-dependent).

The above analysis has assumed an energy- and magnetic field-independent relaxation time. The general theory is by no means limited to such simple cases: the conductivity tensor may be derived from a detailed kinetic theory. This will in general complicate the form of the elements, σ_{ij}, but will not usually affect the symmetry of $\overleftrightarrow{\sigma}$ — that is, whether or not it can be written in the form, Eq. (11). If $\overleftrightarrow{\sigma}$ can be written in this form the analysis of Section III can be carried out.

In the EHL in Ge, the collision processes are dominated by electron-hole collisions, with $\tau \sim 6 \times 10^{-11}$ sec at $B = 0$.[38] In a large magnetic field, there can be structure in σ due to the Shubnikov-deHaas effect. This has been observed in other materials as an approximately sinusoidal

(in 1/B) modulation superimposed on the Alfvén resonances.[39,40] A large magnetic field may directly affect the collision rate: when the cyclotron radius becomes smaller than the screening length, the effective scattering cross section may decrease, enhancing the collision lifetime.[41] These effects will not be further considered further in the present paper, and a constant relaxation rate will be assumed. These modifications should, however, be included when the theory is compared to experiment.

B. Valence Bands

The valence bands in Ge have a doubly degenerate maximum at $\vec{k} = 0$ in the Brillouin zone (ignoring spin). The degeneracy, and the resultant band coupling, greatly complicate the analysis of the conductivity tensor, particularly in a magnetic field.[17] As with the conduction band, these complications are ignored in this paper, and the holes are treated in a semiclassical approximation as two independent particles, one with heavy mass and one light. The band coupling is included only in that the relaxation time is taken to be the same for both types of holes.[25]

In unstressed Ge, the hole masses are treated as scalars, but the values of the masses depend on the field direction.[1] Thus, for heavy holes the conductivity tensor can always be written in the form, Eq. (11), with

$$\sigma_{HHi} = \frac{N_{HH} e^2 \tau_h}{(1 - i\omega\tau_h)} \quad (M_{HHi})^{-1} \quad ,$$

and

$$M^{-1}_{1HH} = \frac{m_{HH}}{m^2_{HH} + \mu^2_h} \qquad \text{(AI.6a)}$$

$$M_{2HH}^{-1} = \frac{-\mu_h}{m_{HH}^2 + \mu_h^2} \tag{AI.6b}$$

$$M_{3HH}^{-1} = m_{HH}^{-1} \tag{AI.6c}$$

with $\mu_h = +|\omega_{co}|\tau_h/(1 - i\omega\tau_h)$. Similar equations hold for the light holes, with $m_{HH} \rightarrow m_{LH}$. Note that because of the opposite sign of electronic charge, μ_e and μ_h have different signs.

Because of the resonant denominators in Eq. (AI.6), the masses are taken to be the cyclotron masses for that direction of magnetic field. The cyclotron masses are in turn found by numerical integration over a constant energy surface, following an approximate technique due to Shockley[42] (see Eq. (74) of Ref. 1):

$$m_c = \frac{\hbar^2}{2\pi} \int \frac{k_\rho d\phi}{\partial E/\partial k_\rho} \Bigg|_{k_z=0} \tag{AI.7}$$

where (z,ρ,ϕ) form a cylindrical coordinate system with the field parallel to z. The mass parameters of Ref. 1 are chosen as A = 13.30, B = 8.92, and C = 11.54, to agree with the experimentally observed cyclotron resonances.[43] That Eq. (AI.6) is only approximate can be clearly seen in the high stress limit. Then the heavy hole mass is ellipsoidal with $m_\ell = 0.04\ m_o$, $m_t = 0.13\ m_o$, and the conductivity tensor should have the same form as (AI.5). In the present approximation, M_1 and M_2 are treated correctly, but $M_3 = m_t$, not m_ℓ as it should. Again, the present form is adequate for exploring the structure expected for Alfvén resonances in a sphere, but a more detailed theory is necessary for comparing the theory to experiment.

The ratio of heavy to light holes, N_{HH}/N_{LL}, is found by numerical integration over the two bands, assuming both have the same Fermi level. In zero stress it is simply equal to $(m_{dHH}/m_{dLH})^{3/2} = 23.6$, where $m_{dHH} = 0.346\ m_o$, $m_{dLH} = 0.042\ m_o$ are the density of states masses of the two bands.

For a weak ⟨111⟩-stress, as in Ge(1:2), the hole masses are complicated functions of angle and stress.[44] In the present paper, it will be assumed that, for Ge(1:2), the splitting of the valence band is small. In particular, the hole masses and heavy-to-light hole density ratio will be taken to be the same as in unstressed Ge.

APPENDIX II: VECTOR SPHERICAL HARMONICS

The vector spherical harmonics, Eqs. (28-30), form a complete set of vector functions over the surface of a sphere. As such, if we perform some vector operation on one of them ($\nabla\times\vec{Y}$, $\hat{z}\hat{z}\cdot\vec{Y}$, etc.), the result can be expressed in terms of other vector spherical harmonics. This is why they are valuable: vector and differential equations can be transformed into matrix equations.

This appendix is essentially a catalog of such transformations, including results found in Refs. 6 and 18. The derivations of these formulas are tedious but straightforward. A good reference on these functions is the book by Edmonds.[45]

These relations are based on the following conventional definition of ordinary spherical harmonics:

$$Y_\ell^m(\theta,\phi) = (-1)^m \left[\frac{(2\ell+1)(\ell-m)!}{4\pi(\ell+m)!}\right]^{\frac{1}{2}} P_\ell^m(\cos\theta)e^{im\phi} \qquad \text{(AII.1)}$$

where $P_\ell^m(x)$ are the associated Legendre polynomials:

$$P_\ell^m(x) = \frac{(1-x^2)^{m/2}}{2^\ell \ell!}\ \frac{d^{\ell+m}}{dx^{\ell+m}}\ (x^2-1)^\ell \qquad \text{(AII.2)}$$

In most derivations, the following form of the vector spherical harmonics is more convenient than the original definition:

$$\vec{Y}^m_{\ell+1,\ell} = \left(\frac{(\ell+m)(\ell+m+1)}{2(\ell+1)(2\ell+1)}\right)^{\frac{1}{2}} Y_\ell^{m-1}\,\hat{e}_1 + \left(\frac{(\ell-m+1)(\ell+m+1)}{(\ell+1)(2\ell+1)}\right)^{\frac{1}{2}} Y_\ell^m\,\hat{e}_0$$
$$+ \left(\frac{(\ell-m)(\ell-m+1)}{2(\ell+1)(2\ell+1)}\right)^{\frac{1}{2}} Y_\ell^{m+1}\,\hat{e}_{-1}$$

$$\vec{Y}^m_{\ell,\ell} = -\left(\frac{(\ell+m)(\ell-m+1)}{2\ell(\ell+1)}\right)^{\frac{1}{2}} Y_\ell^{m-1}\,\hat{e}_1 + \frac{m}{\left(\ell(\ell+1)\right)^{\frac{1}{2}}}\, Y_\ell^m\,\hat{e}_0 + \left(\frac{(\ell-m)(\ell+m+1)}{2\ell(\ell+1)}\right)^{\frac{1}{2}} Y_\ell^{m+1}\,\hat{e}_{-1}$$

$$\vec{Y}^m_{\ell-1,\ell} = \left(\frac{(\ell-m)(\ell-m+1)}{2\ell(2\ell+1)}\right)^{\frac{1}{2}} Y_\ell^{m-1}\,\hat{e}_1 - \left(\frac{(\ell-m)(\ell+m)}{\ell(2\ell+1)}\right)^{\frac{1}{2}} Y_\ell^m\,\hat{e}_0 + \left(\frac{(\ell+m)(\ell+m+1)}{2\ell(2\ell+1)}\right)^{\frac{1}{2}} Y_\ell^{m+1}\,\hat{e}_{-1} \qquad \text{(AII.3)}$$

where the basis vectors, $\hat{e}_i$, are defined in Eq. (44).

These functions are orthonormal

$$\int_0^{2\pi} d\phi \int_0^{\pi} d\theta\, \sin\theta\; \vec{Y}^{m'}_{\ell'+\eta',\ell'} \cdot \vec{Y}^m_{\ell+\eta,\ell} = \delta_{\ell\ell'}\,\delta_{mm'}\,\delta_{\eta\eta'} \qquad \text{(AII.4)}$$

The relations we will need are the following:

DIFFERENTIAL:

Let R(r) be any function of $r = |\vec{r}|$ only. Then

$$\vec{\nabla}\cdot\left(R(r)\vec{Y}^m_{\ell,\ell+1}\right) = -\left(\frac{\ell+1}{2\ell+1}\right)^{\frac{1}{2}} \frac{1}{r^{\ell+2}}\,\frac{d}{dr}\left(R\, r^{\ell+2}\right) Y_\ell^m$$

$$\vec{\nabla}\cdot\left(R\vec{Y}^m_{\ell,\ell}\right) = 0$$

$$\vec{\nabla}\cdot\left(R\vec{Y}^m_{\ell,\ell-1}\right) = \left(\frac{\ell}{2\ell+1}\right)^{\frac{1}{2}} r^{\ell-1}\,\frac{d}{dr}\left(\frac{R}{r^{\ell-1}}\right) Y_\ell^m \qquad \text{(AII.5)}$$

$$\vec{\nabla}\times\left(R\vec{Y}^{m}_{\ell,\ell+1}\right) = i\left(\frac{\ell}{2\ell+1}\right)^{\frac{1}{2}} \frac{1}{r^{\ell+2}} \frac{d}{dr}\left(r^{\ell+2}\, R\right) \vec{Y}^{m}_{\ell,\ell}$$

$$\vec{\nabla}\times\left(R\vec{Y}^{m}_{\ell,\ell}\right) = i\left(\frac{\ell}{2\ell+1}\right)^{\frac{1}{2}} r^{\ell} \frac{d}{dr}\left(\frac{R}{r^{\ell}}\right) \vec{Y}^{m}_{\ell,\ell+1} + i\left(\frac{\ell+1}{2\ell+1}\right)^{\frac{1}{2}} \frac{1}{r^{\ell+1}} \frac{d}{dr}\left(r^{\ell+1}\, R\right) \vec{Y}^{m}_{\ell,\ell-1}$$

$$\vec{\nabla}\times\left(R\vec{Y}^{m}_{\ell,\ell-1}\right) = i\left(\frac{\ell+1}{2\ell+1}\right)^{\frac{1}{2}} r^{\ell-1} \frac{d}{dr}\left(\frac{R}{r^{\ell-1}}\right) \vec{Y}^{m}_{\ell,\ell} \qquad \text{(AII.6)}$$

TENSORIAL:

$$i\hat{z}\times\vec{Y}^{m}_{\ell+1,\ell} = \frac{m}{\ell+1}\vec{Y}^{m}_{\ell+1,\ell} - \left(\frac{\ell(\ell-m+1)(\ell+m+1)}{(\ell+1)^2(2\ell+1)}\right)^{\frac{1}{2}} \vec{Y}^{m}_{\ell,\ell}$$

$$i\hat{z}\times\vec{Y}^{m}_{\ell,\ell} = -\left(\frac{\ell(\ell-m+1)(\ell+m+1)}{(\ell+1)^2(2\ell+1)}\right)^{\frac{1}{2}} Y^{m}_{\ell+1,\ell} + \frac{m}{\ell(\ell+1)}\vec{Y}^{m}_{\ell,\ell} - \left(\frac{(\ell+1)(\ell-m)(\ell+m)}{\ell^2(2\ell+1)}\right)^{\frac{1}{2}} \vec{Y}^{m}_{\ell-1,\ell}$$

$$i\hat{z}\times\vec{Y}^{m}_{\ell-1,\ell} = -\left(\frac{(\ell+1)(\ell-m)(\ell+m)}{\ell^2(2\ell+1)}\right)^{\frac{1}{2}} \vec{Y}^{m}_{\ell,\ell} - \frac{m}{\ell}\vec{Y}^{m}_{\ell-1,\ell} \qquad \text{(AII.7)}$$

$$\hat{z}\hat{z}\cdot\vec{Y}^{m}_{\ell+1,\ell} = \frac{(\ell-m+1)(\ell+m+1)}{(\ell+1)(2\ell+1)}\vec{Y}^{m}_{\ell+1,\ell} + m\left(\frac{(\ell-m+1)(\ell+m+1)}{\ell(\ell+1)^2(2\ell+1)}\right)^{\frac{1}{2}} \vec{Y}^{m}_{\ell,\ell} - \left(\frac{(\ell-m+1)(\ell+m+1)(\ell^2-m^2)}{\ell(\ell+1)(2\ell+1)^2}\right)^{\frac{1}{2}} \vec{Y}^{m}_{\ell-1,\ell} \qquad \text{(AII.8a)}$$

$$\hat{z}\hat{z} \cdot \vec{Y}^m_{\ell,\ell} = m\left(\frac{(\ell-m+1)(\ell+m+1)}{\ell(\ell+1)^2\,(2\ell+1)}\right)^{\frac{1}{2}} \vec{Y}^m_{\ell+1,\ell} + \frac{m^2}{\ell(\ell+1)}\,\vec{Y}^m_{\ell,\ell}$$

$$- m\left(\frac{\ell^2-m^2}{\ell^2(\ell+1)(2\ell+1)}\right)^{\frac{1}{2}} \vec{Y}^m_{\ell-1,\ell} \qquad \text{(AII.8b)}$$

$$\hat{z}\hat{z} \cdot \vec{Y}^m_{\ell-1,\ell} = \left(\frac{(\ell-m+1)(\ell+m+1)(\ell^2-m^2)}{\ell(\ell+1)\,(2\ell+1)^2}\right)^{\frac{1}{2}} \vec{Y}^m_{\ell+1,\ell}$$

$$- \left(\frac{(\ell-m)(\ell+m+1)(\ell^2-m^2)}{2\ell^2(\ell+1)(2\ell+1)}\right)^{\frac{1}{2}} \vec{Y}^m_{\ell,\ell} + \frac{\ell^2-m^2}{\ell(2\ell+1)}\,\vec{Y}^m_{\ell-1,\ell} \qquad \text{(AII.8c)}$$

$$\hat{r} \cdot \vec{Y}^m_{\ell,\ell-1} = \left(\frac{\ell}{2\ell+1}\right)^{\frac{1}{2}} Y^m_\ell$$

$$\hat{r} \cdot \vec{Y}^m_{\ell,\ell} = 0$$

$$\hat{r} \cdot \vec{Y}^m_{\ell,\ell+1} = -\left(\frac{\ell+1}{2\ell+1}\right)^{\frac{1}{2}} Y^m_\ell \qquad \text{(AII.9)}$$

$$\hat{r} \times \vec{Y}^m_{\ell,\ell-1} = i\left(\frac{\ell+1}{2\ell+1}\right)^{\frac{1}{2}} \vec{Y}^m_{\ell,\ell}$$

$$\hat{r} \times \vec{Y}^m_{\ell,\ell} = i\left[\left(\frac{\ell}{2\ell+1}\right)^{\frac{1}{2}} \vec{Y}^m_{\ell,\ell+1} + \left(\frac{\ell+1}{2\ell+1}\right)^{\frac{1}{2}} \vec{Y}^m_{\ell,\ell-1}\right]$$

$$\hat{r} \times \vec{Y}^m_{\ell,\ell+1} = i\left(\frac{\ell}{2\ell+1}\right)^{\frac{1}{2}} \vec{Y}^m_{\ell,\ell} \qquad \text{(AII.10)}$$

Finally, we can find the action of an arbitrary tensor element on $\vec{Y}\ (\hat{e}_i\hat{e}_j \cdot \vec{Y})$. If we rewrite Eq. (AII.3) as

$$\vec{Y}^m_{\ell+j,\ell} = \sum_i \hat{e}_i\ Y^{m-i}_\ell\ c_{\ell,m,j,i} \tag{AII.11}$$

this can be inverted to give

$$\hat{e}_i\ Y^m_\ell = \sum_j \vec{Y}^{m+i}_{\ell+j,\ell}\ c_{\ell,m+i,j,i} \tag{AII.12}$$

These two equations can then be combined to yield

$$\hat{e}_i\hat{e}_j \cdot \vec{Y}^m_{\ell+\eta,\ell} = c_{\ell,m,\eta,j} \sum_\nu c_{\ell,m+i-j,\nu,i}\ \vec{Y}^{m+i-j}_{\ell+\nu,\ell} \tag{AII.13}$$

The above relations can be rewritten in terms of the $\vec{A}^m_\ell$, $\vec{B}^m_\ell$, $\vec{C}^m_\ell$. The most difficult is perhaps Eq. (AII.8), which results in

$$\begin{aligned}\hat{z}\hat{z} \cdot \vec{C}^m_\ell &= \frac{m^2}{\ell(\ell+1)}\ \vec{C}^m_\ell + \frac{m}{[\ell(\ell+1)]^{1/2}}\left[\left(\frac{(\ell-m+1)(\ell+m+1)}{(2\ell+1)(2\ell+3)}\right)^{1/2}\ \vec{B}^m_{\ell+1}\right. \\ &- \left(\frac{(\ell-m)(\ell+m)}{(2\ell+1)(2\ell-1)}\right)^{1/2}\ \vec{B}^m_{\ell-1} - \left(\frac{(\ell-m+1)(\ell+m+1)(\ell+2)}{(\ell+1)(2\ell+1)(2\ell+3)}\right)^{1/2}\ \vec{A}^m_{\ell+1} \\ &- \left.\left(\frac{(\ell+m)(\ell-m)(\ell-1)}{\ell(2\ell+1)(2\ell-1)}\right)^{1/2}\ \vec{A}^m_{\ell-1}\right] \\ &\equiv \sum_{\ell'}\left(V^3_{1\ell\ell'}\ \vec{A}^m_{\ell'} + V^3_{2\ell\ell'}\ \vec{B}^m_{\ell'} + V^3_{3\ell\ell'}\ \vec{C}^m_{\ell'}\right)\end{aligned} \tag{AII.14a}$$

$$\hat{z}\hat{z}\cdot\vec{A}^m_\ell = -\frac{m}{\ell+1}\left(\frac{\ell(\ell-m+1)(\ell+m+1)}{(\ell+2)(2\ell+1)(2\ell+3)}\right)^{\frac{1}{2}}\vec{C}^m_{\ell+1} - \frac{m}{\ell}\left(\frac{(\ell+1)(\ell^2-m^2)}{((2\ell)^2-1)(\ell-1)}\right)^{\frac{1}{2}}\vec{C}^m_{\ell-1}$$

$$-\frac{1}{2\ell+3}\left(\frac{\ell(\ell+m+1)(\ell-m+1)(\ell+m+2)(\ell-m+2)}{(2\ell+1)(\ell+1)(\ell+2)(2\ell+5)}\right)^{\frac{1}{2}}$$

$$\times\left[\sqrt{\ell-2}\ \vec{B}^m_{\ell+2} - \sqrt{\ell+3}\ \vec{A}^m_{\ell+2}\right] + \frac{1}{2\ell-1}\left(\frac{(\ell+1)(\ell^2-m^2)(\ell+m-1)(\ell-m-1)}{\ell(2\ell+1)(\ell-1)(2\ell-3)}\right)^{\frac{1}{2}}$$

$$\times\left[\sqrt{\ell-2}\ \vec{A}^m_{\ell-2} + \sqrt{\ell-1}\ \vec{B}^m_{\ell-2}\right] + \frac{1}{2\ell+1}\left[\frac{(\ell+m+1)(\ell-m+1)}{(\ell+1)(2\ell+2)}\right.$$

$$\left.\times\left(\ell\,\vec{A}^m_\ell + \sqrt{\ell(\ell+1)}\ \vec{B}^m_\ell\right) + \frac{\ell^2-m^2}{(2\ell-1)}\left((\ell+1)\,\vec{A}^m_\ell - \sqrt{\ell(\ell+1)}\ \vec{B}^m_\ell\right)\right]$$

$$\equiv \sum_{\ell'}\left(V^1_{1\ell\ell'}\,\vec{A}^m_{\ell'} + V^1_{2\ell\ell'}\,\vec{B}^m_{\ell'} + V^1_{3\ell\ell'}\,\vec{C}^m_{\ell'}\right) \qquad \text{(AII.14b)}$$

$$\hat{z}\hat{z}\cdot\vec{B}^m_\ell = \frac{-m}{\sqrt{\ell+1}}\left(\frac{(\ell+m+1)(\ell-m+1)}{(2\ell+1)(\ell+2)(2\ell+3)}\right)^{\frac{1}{2}}\vec{C}^m_{\ell+1} + \frac{m}{\sqrt{\ell}}\left(\frac{\ell^2-m^2}{(2\ell+1)(\ell-1)(2\ell-1)}\right)^{\frac{1}{2}}\vec{C}^m_{\ell-1}$$

$$-\left(\frac{(\ell+m+1)(\ell-m+1)(\ell-m+2)(\ell+m+2)}{(2\ell+3)^2(2\ell+1)(\ell+2)(2\ell+5)}\right)^{\frac{1}{2}}\left[\sqrt{\ell+2}\ \vec{B}^m_{\ell+2} - \sqrt{\ell+3}\ \vec{A}^m_{\ell+2}\right]$$

$$-\left(\frac{(\ell+m-1)(\ell-m-1)(\ell^2-m^2)}{(2\ell-1)^2(2\ell+1)(\ell-1)(2\ell-3)}\right)^{\frac{1}{2}}\left[\sqrt{\ell-2}\ \vec{A}^m_{\ell-2} + \sqrt{\ell-1}\ \vec{B}^m_{\ell-2}\right]$$

$$+\frac{1}{2\ell+1}\left[\frac{(\ell+m+1)(\ell-m+1)}{(\ell+1)(2\ell+3)}\left[\left(\ell(\ell+1)\right)^{\frac{1}{2}}\vec{A}^m_\ell + (\ell+1)\,\vec{B}^m_\ell\right]\right.$$

$$\left.+\frac{\ell^2-m^2}{\ell(2\ell-1)}\left[\ell\vec{B}^m_\ell - \left(\ell(\ell+1)\right)^{\frac{1}{2}}\vec{A}^m_\ell\right]\right]$$

$$\equiv \sum_{\ell'}\left(V^2_{1\ell\ell'}\,\vec{A}^m_{\ell'} + V^2_{2\ell\ell'}\,\vec{B}^m_{\ell'} + V^2_{3\ell\ell'}\,\vec{C}^m_{\ell'}\right) \qquad \text{(AII.14c)}$$

APPENDIX III. DETAILS OF EXACT SOLUTION (SECTION III)

A) The relation $\vec{J} = (\overleftrightarrow{\sigma} - \frac{i\omega\varepsilon_L}{4\pi})\cdot\vec{E}$

can be inverted:

$$\vec{E} = \overleftrightarrow{\rho}' \cdot \vec{J} \tag{AIII.1}$$

$$\overleftrightarrow{\rho}' = \begin{pmatrix} \rho_1' & i\rho_2' & 0 \\ -i\rho_2' & \rho_1' & 0 \\ 0 & 0 & \rho_3' \end{pmatrix} \tag{AIII.2}$$

where

$$\rho_1' = \sigma_1'/(\sigma_1'^2 - \sigma_2^2) \tag{AIII.3a}$$

$$\rho_2' = -\sigma_2/(\sigma_1'^2 - \sigma_2^2) \tag{AIII.3b}$$

$$\rho_3' = \left[\sigma_3 - \frac{i\omega\varepsilon_L}{4\pi}\right]^{-1} \tag{AIII.3c}$$

and

$$\sigma_1' = \sigma_1 - \frac{i\omega\varepsilon_L}{4\pi} \tag{AIII.3d}$$

By substituting Eq. (AIII.1) into Eq. (7), we find

$$\vec{\nabla} \times \{\vec{\nabla} \times [\vec{J} + \gamma\hat{z}\hat{z} \cdot \vec{J} + Wz \times \vec{J}]\} = q_o^2 \vec{J} \tag{AIII.4}$$

where

$$q_o^2 = \frac{4\pi i\omega}{\rho_1' c^2} \tag{AIII.5a}$$

$$\gamma = (\rho_3' - \rho_1')/\rho_1' \tag{AIII.5b}$$

$$W = -i\rho_2'/\rho_1' = i\sigma_2/\sigma_1' \qquad \text{(AIII.5c)}$$

B) The eigenvalue equation.

By substituting J_q (Eq. 32) into Eq. (AIII.4), and utilizing the relations of Appendix II, this differential equation can be turned into a linear equation relating the various $\vec{A}_{\ell m}$, $\vec{C}_{\ell m}$:

$$\sum_{\ell m} q^2 \Big[(a_{\ell m}\vec{A}^m_\ell + c_{\ell m}\vec{C}^m_\ell) +$$

$$+ \gamma \sum_{\ell'} \Big\{(a_{\ell m}V^1_{1\ell\ell'} + c_{\ell m}V^3_{1\ell\ell'})\vec{A}^m_{\ell'} + (a_{\ell m}V^1_{3\ell\ell'} + c_{\ell m}V^3_{3\ell\ell'})\vec{C}^m_{\ell'}\Big\}$$

$$- \Big\{iW \frac{m}{\ell(\ell+1)}(a_{\ell m}\vec{A}^m_\ell + c_{\ell m}\vec{C}^m_\ell) + \sum_{\ell'} M^m_{\ell\ell'}(a_{\ell m}\vec{C}^m_{\ell'} - c_{\ell m}\vec{A}^m_{\ell'})\Big\}\Big]$$

$$= q_0^2 \sum_{\ell m} (a_{\ell m}\vec{A}^m_\ell + c_{\ell m}\vec{C}^m_\ell) \qquad \text{(AIII.6)}$$

Here the V's are defined in Eq. (AII.14),

$$M^m_{\ell,\ell-1} = -M^m_{\ell-1,\ell} = \left(\frac{(\ell+1)(\ell-1)(\ell-m)(\ell+m)}{\ell^2(2\ell-1)(2\ell+1)}\right)^{1/2}, \qquad \text{(AIII.7)}$$

and $M^m_{\ell\ell'} = 0$ if $\ell' \neq \ell \pm 1$. Since the $\vec{A}_{\ell m}$'s and $\vec{C}_{\ell m}$'s are mutually orthogonal, the coefficient of each must vanish separately in Eq. (AIII.6). By rewriting

$$q^2 = \frac{q_0^2}{(1-\lambda)} \ , \qquad \text{(AIII.8)}$$

Eq. (AIII.6) is transformed into the eigenvalue equations:

$$\gamma[a_{\ell m} V^1_{1\ell,\ell} + a_{\ell+2,m} V^1_{1,\ell+2,\ell} + a_{\ell-2,m} V^1_{1,\ell-2,m} + c_{\ell+1,m} V^3_{1,\ell+1,\ell} + c_{\ell-1,m} V^3_{1,\ell-1,\ell}]$$

$$-iW \left[\frac{m}{\ell(\ell+1)} a_{\ell m} - c_{\ell+1,m} M^m_{\ell+1,\ell} - c_{\ell-1,m} M^m_{\ell-1,\ell}\right] = -\lambda a_{\ell m} \qquad \text{(AIII.9)}$$

$$\gamma[c_{\ell m} V^3_{3\ell,\ell} + a_{\ell+1,m} V^1_{3,\ell+1,m} + a_{\ell-1,m} V^1_{3,\ell-1,m}]$$

$$\text{(AIII.10)}$$

$$-iW \left[\frac{m}{\ell(\ell+1)} c_{\ell m} - a_{\ell+1,m} M^m_{\ell+1,\ell} - a_{\ell-1,m} M^m_{\ell-1,\ell}\right] = -\lambda c_{\ell m}$$

These equations are solved numerically. Once $\vec{J}_q$ is known, the electric and magnetic fields can readily be found, using Eqs. (2d) and (AIII.1). The magnetic field may be expressed

$$\vec{B}_q = \frac{-4\pi i}{qc} \sum_{\ell m} (c_{\ell m} \vec{A}^m_\ell - a_{\ell m} \vec{C}^m_\ell) \qquad \text{(AIII.11)}$$

while the electric field may be expressed as

$$\vec{E}_q = (1-\lambda)\ \rho'_1\ \vec{J}_q + \sum_{\ell m} f'_{\ell m}\ \vec{B}^m_\ell \qquad \text{(AIII.12)}$$

where the $f'_{\ell m}$ are defined through

$$f'_{\ell m} = \frac{f_{\ell m} + (\ell+1)\ \rho'_1 a_{\ell m}(1-\lambda)}{\sqrt{\ell(\ell+1)}} \tag{AIII.13}$$

$$f_{\ell m}/\rho'_1 = iW\left[m\,\frac{\ell+1}{\ell}\,a_{\ell m} - (2\ell+1)\ M^m_{\ell-1,\ell}\ c_{\ell-1,m}\right] \tag{AIII.14}$$

$$+\ \gamma\left[\delta_\ell\left(V^3_{2,\ell-1,\ell}c_{\ell-1,m} + V^1_{2,\ell-2,\ell}\ a_{\ell-2,m}\right) - \frac{(\ell^2-m^2)(\ell+1)}{\ell(2\ell-1)}\ a_{\ell m}\right]$$

$$\delta_\ell = (2\ell+1)\ \sqrt{(\ell+1)/\ell} \tag{AIII.15}$$

REFERENCES

1. G. Dresselhaus, A. F. Kip, and C. Kittel, Phys. Rev. 98, 368 (1955).

2. Cyclotron resonance can, however, be observed in metals, as suggested by M. I. Azbel and E. A. Kaner, Zh. Eksp. Teor. Fiz. 30, 811 (1956); [Sov. Phys. - JETP 3, 772 (1956)].

3. G. Dresselhaus, A. F. Kip, and C. Kittel, Phys. Rev. 100, 618 (1955).

4. For general reviews on these topics, see B. W. Maxfield, Am. J. Phys. 37, 241 (1969); A. C. Baynham and A. D. Boardman, Plasma Effects in Semiconductors: Helicon and Alfvén Waves (Taylor & Francis, London, 1971), reprinted from Adv. in Phys. 19, 575 (1970); E. A. Kaner and V. G. Skobov, Plasma Effects in Metals: Helicon and Alfvén Waves (Taylor & Francis, London, 1971), reprinted from Adv. in Phys. 17, 605 (1968).

5. For recent treatments of Mie scattering, see M. Born and E. Wolf, Principles of Optics (Fourth Ed.) Pergamon, Oxford (1970), Section 13.5; and H. C. van de Hulst, Light Scattering by Small Particles, Wiley, New York (1957).

6. G. W. Ford and S. A. Werner, Phys. Rev. B8, 3702 (1973).

7. R. S. Markiewicz, J. P. Wolfe, and C. D. Jeffries, Phys. Rev. Lett. 32, 1357 (1974), and 34, 59(E) (1975).

8. J. P. Wolfe, R. S. Markiewicz, C. Kittel, and C. D. Jeffries, Phys. Rev. Lett. 34, 275 (1975).

9. For reviews of the properties of electron-hole drops, see Ya. E. Pokrovskii, Phys. Stat. Sol. (a) 11, 385 (1972); C. D. Jeffries, Science 189, 955 (1975); J. C. Hensel, T. G. Phillips, and G. A. Thomas, Solid State Physics (to be published); and T. M. Rice,

Solid State Physics, (to be published).

10. V. S. Bagaev, N. V. Zamkovets, L. V. Keldysh, N. N. Sibeldin, and V. A. Tsvetkov, Zh. Eksp. Teor. Fiz. 70, 1501 (1976). [Sov. Phys. - JETP 43, 783 (1976)].
11. H. Numata, J. Phys. Soc. Japan 36, 309 (1974).
12. R. S. Markiewicz, thesis, Univ. of California at Berkeley (1975), unpublished.
13. J. P. Wolfe, R. S. Markiewicz, and C. D. Jeffries, Proc. 3rd Intern. Conf. on Light Scattering in Solids, Campinas (Flammarion and Springer-Verlag, Paris, 1975), p. 173.
14. R. S. Markiewicz, J. P. Wolfe, and C. D. Jeffries, Phys. Rev. B 15, 1988 (1977).
15. J. P. Wolfe, R. S. Markiewicz, S. M. Kelso, J. E. Furneaux, and C. D. Jeffries, to be published.
16. M. Cardona and B. Rosenblum, Phys. Rev. 129, 991 (1963).
17. A. C. Beer, "Galvanomagnetic Effects in Semiconductors," Solid State Physics, Supp. 4, edited by F. Seitz and D. Turnbull, Academic Press, N.Y. (1963).
18. G. W. Ford, J. K. Furdyna, and S. A. Werner, Phys. Rev. B 12, 1452 (1975).
19. Galeener refined the theory and corrected an error in the definition of the γ_{ij}. See F. L. Galeener, thesis, Purdue Univ. (1970) - available on University microfilms #71-2599; F. L. Galeener and J. K. Furdyna, Phys. Rev. B4, 1853 (1971); F. L. Galeener, T. A. Evans, and J. K. Furdyna, Phys. Rev. Lett. 29, 728 (1972); T. A. Evans and J. K. Furdyna, Phys. Rev. B8, 1461 (1973).

20. A similar comparison was given, for the helicon case, in R. S. Markiewicz, Phys. Rev. B 10, 1766 (1974).

21. In earlier calculations, (Refs. 6,12) it was assumed that, e.g. an electric source excited only electric multipoles outside the sphere - that is, $F^m_{2\ell} = 0$ if $D_{Bm} = 0$; similarly $F^m_{1\ell} = 0$ if $D_{Em} = 0$. This assumption altered the form of the R-matrices. This error is not serious for the magnetic dipole case, since the terms in error (Eq. 55a) can, to lowest order in $k_o a = \sqrt{\varepsilon_L}\ \frac{\omega a}{c}$, be written as

$$R_{E\ell q} \simeq \frac{-4\pi i \ell}{\omega \varepsilon^o_L} a_{\ell m} \frac{j_\ell(qa)}{qa} ,$$

which is the previous result (Ref.6). I thank G. W. Ford and S. A. Werner for pointing out the need to include both $F^m_{1\ell}$ and $F^m_{2\ell}$.

22. F. B. Hildebrand, Methods of Applied Mathematics, (Second Ed.), Prentice-Hall, Englewood Cliffs, N.J. (1965), section 1.4.

23. G. W. Ford and S. A. Werner, to be published.

24. P. B. Visscher and L. M. Falicov, Phys. Rev. B 2, 1518 (1970).

25. A model commonly used in studying valence band mobility is to treat the holes as decoupled, except that they have the same collision time $\tau_{LH} = \tau_{HH}$. See J. D. Wiley, in Semiconductor and Semimetals, Vol. 10, R. K. Willardson & A. C. Beer (Eds), Academic Press, N.Y. (1975), p.91.

26. P. Vashishta, S. G. Das, and K. S. Singwi, Phys. Rev. Lett. 33, 911 (1974).

27. The identification is herein made that the resonances related to σ_+ in the empirical Mie theory should be compared to the TM+

resonances of the exact theory. In this case, the EMT would predict no LM resonances.

28. In Figs. 4-6, the anticrossing behavior in these weaker modes is not studied in detail: the theoretical curves follow the peak of the intensity rather than the individual resonance lines.

29. In EMT, these lines do not pass exactly through the origin, but within a few hundred Gauss of it. See Fig. IV 2 of Ref. 12.

30. This saturation was noted in J. R. Dixon, Jr. and J. K. Furdyna, Phys. Rev. B 13, 4626 (1976).

31. For Ge(4:2) m_e is the average of the cyclotron mass in the four valleys.

32. The Rayleigh limit resonances were discussed for EHD in unstressed Ge ($B \parallel \langle 100 \rangle$ or $\langle 111 \rangle$) by J. R. Dixon, Jr. and J. K. Furdyna, Phys. Rev. B 13, 3657 (1976).

33. In Ref. 6, due to a simplifying assumption, all resonances did have the same Rayleigh limit, and this behavior was indeed observed. See Ref. 20.

34. This assumes $\omega\tau \ll 1$.

35. R. E. Michel and B. Rosenblum, Phys. Rev. 128, 1646 (1962).

36. T. Sanada, T. Ohyama, and E. Otsuka, Sol. St. Comm. 12, 1201 (1973).

37. P. R. Wallace, Can. J. Phys. 43, 2162 (1965) and 44, 2495 (1966).

38. T. Ohyama, A. D. A. Hansen, and J. L. Turney, Sol. St. Comm. 19, 1083 (1976); A. S. Kaminskii, Ya. E. Pokrovskii and A. E. Zhudkov, Zh. Eksp. Teor. Fiz. 72, 1960 (1977).

39. G. A. Williams and G. E. Smith, IBM Journal of R.&D. 8, 276 (1964).

40. S. Feser, thesis, Univ. of British Columbia (1975), unpublished, esp. p. 98.

41. For related results in ionized impurity scattering, see S. C. Miller and M. A. Omar, Phys. Rev. 123, 74 (1961).

42. W. Shockley, Phys. Rev. 79, 191 (1950).

43. J. P. Wolfe, R. S. Markiewicz, unpublished.

44. I. Balslev, Phys. Rev. 143, 636 (1966).

45. A. R. Edmonds, Angular Momentum in Quantum Mechanics, Princeton University Press, Princeton, N.J. (1957).

FIGURE CAPTIONS

Fig. 1. Magnetic dipole resonant field distributions. The figure shows the electric and magnetic fields induced in a sphere by the frequency-dependent field $\vec{B}_1$ in the presence of a static field, $\vec{B}_o$, for the transverse case $\vec{B}_1 \perp \vec{B}_0$. The field distribution is actually calculated for an isotropic sphere, and it is hypothesized that (for a small enough sphere) this distribution is not changed greatly by the static field $\vec{B}_o$. Fields near the two lowest dipole resonances are shown. Below each sphere is shown the intensity and direction of the induced electric field along a diagonal of the sphere perpendicular to $\vec{B}_1$. From this, the concept of fitting one (or two) wavelengths inside the sphere should be clear.

Fig. 2. Magnetic dipole absorption for a sphere of EHL (Ge(1:2)) inside bulk Ge: Microwave power absorption as a function of field for several values of drop radius a, B ∥ ⟨111⟩. (Top) LM: The microwave field $\vec{B}_1$ is parallel to the static field; (center) TM+ and (bottom) TM-: the microwave field is circularly polarized perpendicular to $\vec{B}$. The actual power absorbed depends on the magnitude of $\vec{B}_1$, and can be inferred from Fig. 4. All the spectra in Fig. 2 are drawn to a common scale (fixed value of $|\vec{B}_1|$). The more intense lines of each spectrum are labelled.

Fig. 3. Magnetic dipole absorption for Ge(1:2): resonant field versus drop radius. The material parameters and the labelling of the modes is the same as in Fig. 2. Many weaker resonances are not shown, for clarity. The solid lines are the resonant fields calculated for the exact theory of Section III, while the dashed lines represent the approximate theory of Section IV. The dots in Fig. (3a) for a=200 μm represent the spacing of resonances predicted by the EMT. The arrows in all figures at a=0 represent the approximate Rayleigh limit fields calculated in Section V.C.

Fig. 4. Magnetic dipole absorption for Ge(1:2): Absorption intensity versus drop radius. What is plotted is actually the magnetic susceptibility, χ'', defined in Eq. (78). The solid curves represent the labelled resonances of the exact theory, where the labelling is the same as in Figs. 2 and 3. The dashed lines represent the approximate theory, as in Fig. 3. The evidence of mode crossing is especially strong here: the sum of the peak intensities of all the labelled resonances (plotted as a dotted line) is almost equal to the intensity of the single resonance of the approximate theory. Note that for small drops, χ'' increases as a^2 (the absorbed power increases like a^5).

Fig. 5. Magnetic dipole absorption for Ge(1:2): Linewidth (full width at half maximum intensity) versus resonant fields. Again the solid lines represent the result of the exact theory, and the dashed lines represent the approximate theory. While there is much evidence of mode crossing, the resonance width generally increases linearly with B, except at the lowest fields.

Fig. 6. Magnetic dipole absorption for EHD in Ge: resonant field versus drop radius: (top) Ge(4:2), B ∥ ⟨100⟩; (center) Ge(4:2), B ∥ ⟨111⟩; (bottom) Ge(1:1), B ∥ ⟨111⟩. The LM resonances are indicated by solid lines, the TM+ by dashed, and the TM- by dotted lines. Only the most intense resonances, corresponding to the labelled resonances of Fig. (2), are shown.

Fig. 7. Induced field distribution for multipole absorption. These fields were calculated as in Fig. (1), and represent the approximate field distributions near the lowest magnetic dipole, quadrupole, and octupole resonances. The upper figures show the magnetic field distribution in a central plane section of the sphere. The lower figures show the electric field distribution on a spherical shell.

Fig. 8. Angle dependence of the dimensional resonances in EHD. (Top) Ge(1:2); (center) Ge(4:2); (bottom) Ge(1:1). These resonances were calculated using the approximate theory, for a drop with a = 40μm. The field is assumed to lie in a $(01\bar{1})$-plane, with θ being the angle between the field direction and the ⟨100⟩-axis. The results of the exact theory are also shown along the high symmetry of directions where this theory is

applicable: The LM resonance is indicated by a 0, the TM+ by a + sign, and the TM- by a -. (For Ge(4:2), there are already two TM+(TM-) resonances of comparable intensity, and the fields of both are shown).

Fig. 9. Angle dependence of the dimensional resonances in Ge(1:2). Top: Rayleigh limit (a=1μm). In addition to the calculations of the approximate theory (solid lines), the results of the elementary considerations of Section V.C are presented as dashed lines. Curve 1 represents cyclotron resonance for a particle with mass $2m_e$; curve 2 is for mass $2m_h$; curve 3 for mass $2m_r$. Bottom: Large drop case (a=120μm). The dashed curve is proportional to $\sqrt{m_e+m_h}$, as explained in the text.

Fig. 10. Electric dipole absorption for Ge(1:2): power absorbed versus field for several drop sizes. All the spectra are drawn to a common scale; for easy comparison with Fig. (2), it is assumed that $|E_1|^2$ here has the same value as $|B_1|^2$ in that figure.

Fig. 11. Electric dipole absorption for Ge(1:2): resonant field versus drop radius. The labelling of modes is the same here as in Fig. 10. For simplicity, the complicated series of line crossings associated with the a-mode in Fig. 11(c) will not be considered in detail.

Fig. 12. Electric dipole absorption for Ge(1:2): electric susceptibility, χ'', versus drop radius. The electric susceptibility is defined by an equation analogous to Eq. (78), with $\vec{B}_1 \rightarrow \vec{E}_1$. For small drops, this susceptibility changes quite rapidly with a; for example $\chi'' \propto a^4$, a^8 for the a- and b-modes of Fig. 12a. In Fig. 12c, certain mode-crossings associated with the a- and b-modes have been neglected, and the corresponding regions of the curves are shown as dashed.

Fig. 13. Electric dipole absorption for Ge(1:2): linewidth versus resonant field. The labelling of the modes is the same as in Figs. 10, 11, and 12. As in the magnetic dipole case (Fig. 5), the linewidth increases approximately linearly in B.

Fig. 14. Electric dipole absorption for EHD in Ge: resonant field versus drop radius. Top: Ge(4:2), B $\parallel$ ⟨100⟩; center: Ge(4:2), B $\parallel$ ⟨111⟩; bottom: Ge(1:1), B $\parallel$ ⟨111⟩. Only the most intense resonances, corresponding to the labelled resonances of Fig. (10), are shown.

Fig. 15. Angular dependence of the low-field, approximately size-independent resonances, Ge(4:2). The angles are defined as in Figs. 8 and 9, but, because of the symmetry in Ge(4:2), only half of the spectrum needs to be presented. These resonances occur in both the electric and magnetic dipole absorption, at nearly the same fields.

Fig. 16. Transition from Alfvén to helicon resonances by increasing the hole mass. (16a). Resonant field versus m_h for Rayleigh limit resonances (a=1μm). (16b) Resonant fields versus drop radius for $m_h = 20\ m_e$. Dashed curve shows the TM+ resonance in the helicon limit. (16c) Linewidth versus magnetic field for the TM+ resonance, $m_h = 20\ m_e$.

Fig. 17. Transition from Alfvén to helicon resonances by decreasing the hole concentration. Plot shows resonant fields versus drop radius for $n_h = \frac{1}{2}\ n_e$.

Fig. 18. Transition from Alfvén to helicon resonances by increasing the hole scattering rate. Plot shows linewidth of TM+ resonance as a function of $\omega\tau_h$, for a = 20 μm.

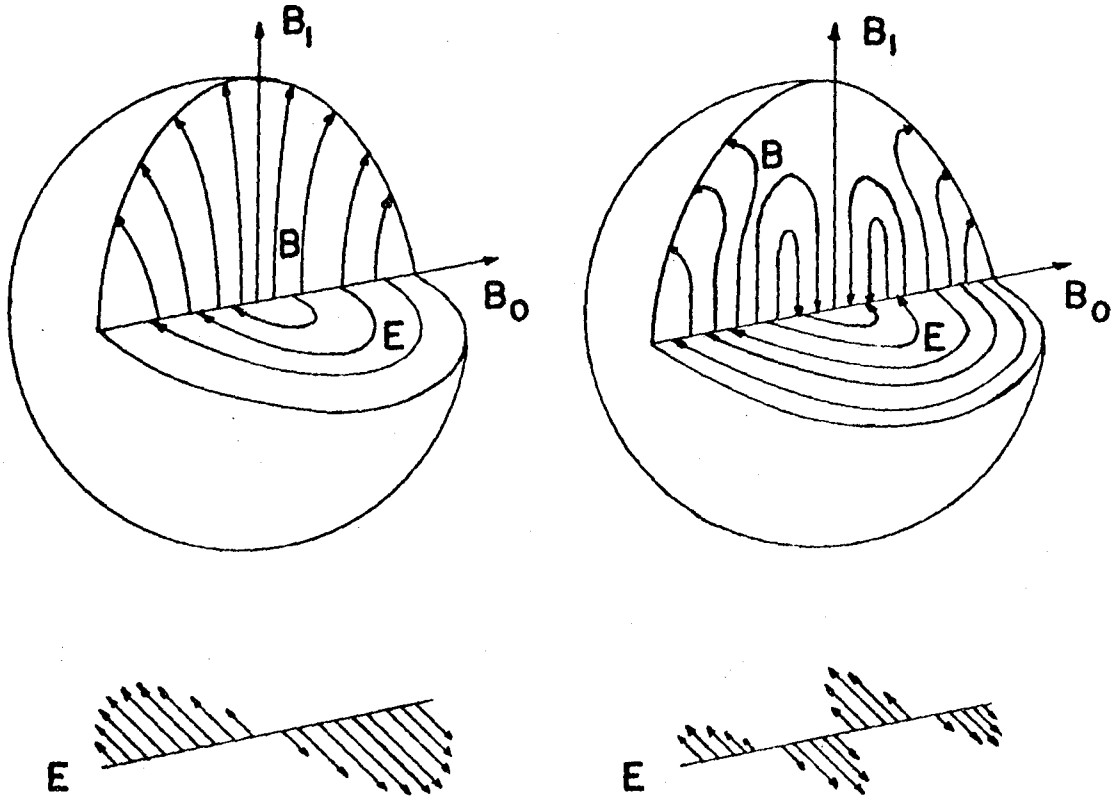

Dipole
j = 1

Dipole
j = 2

XBL 7710-10075

Fig. 1

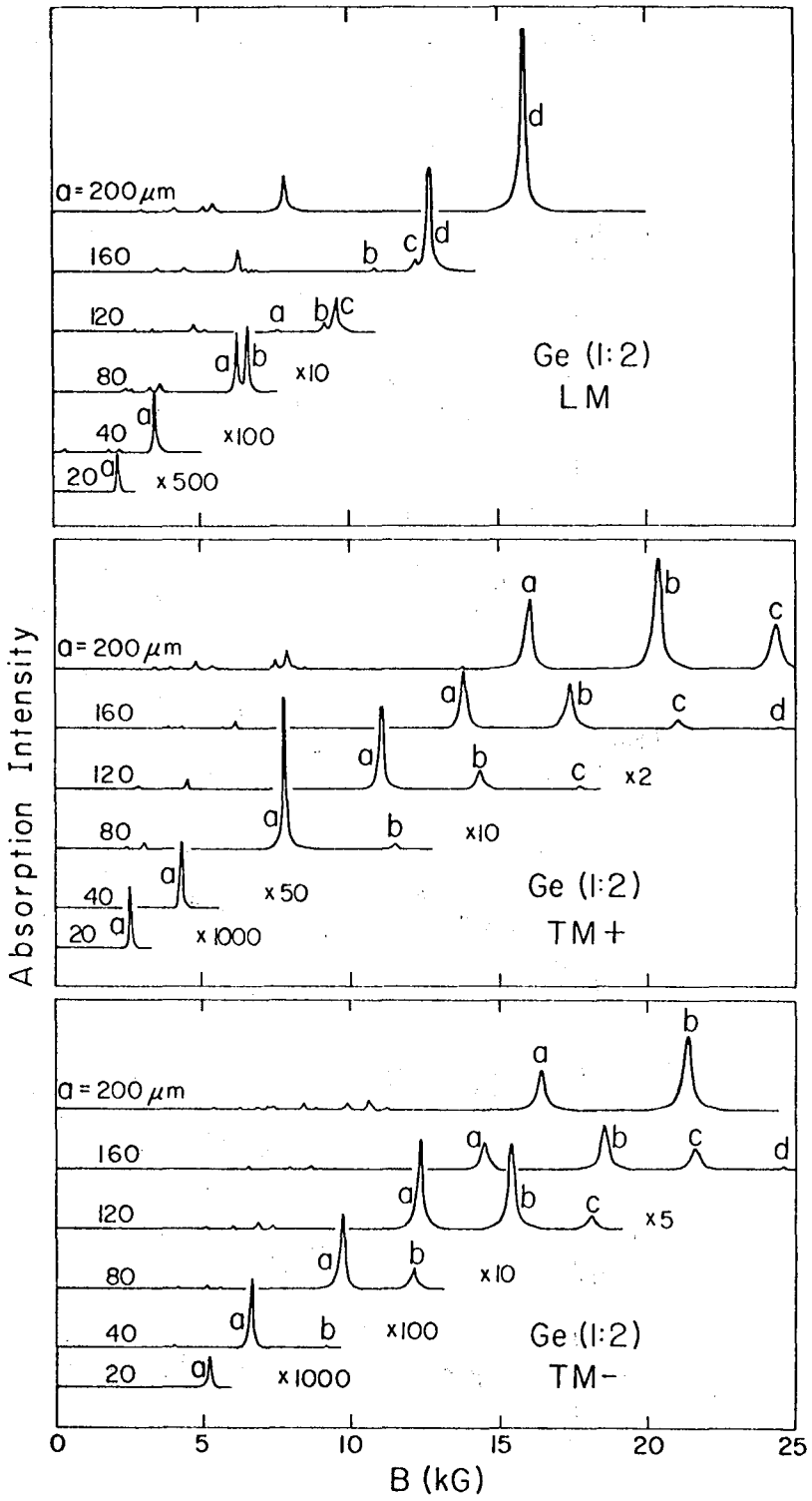

XBL 7710-6207

Fig. 2

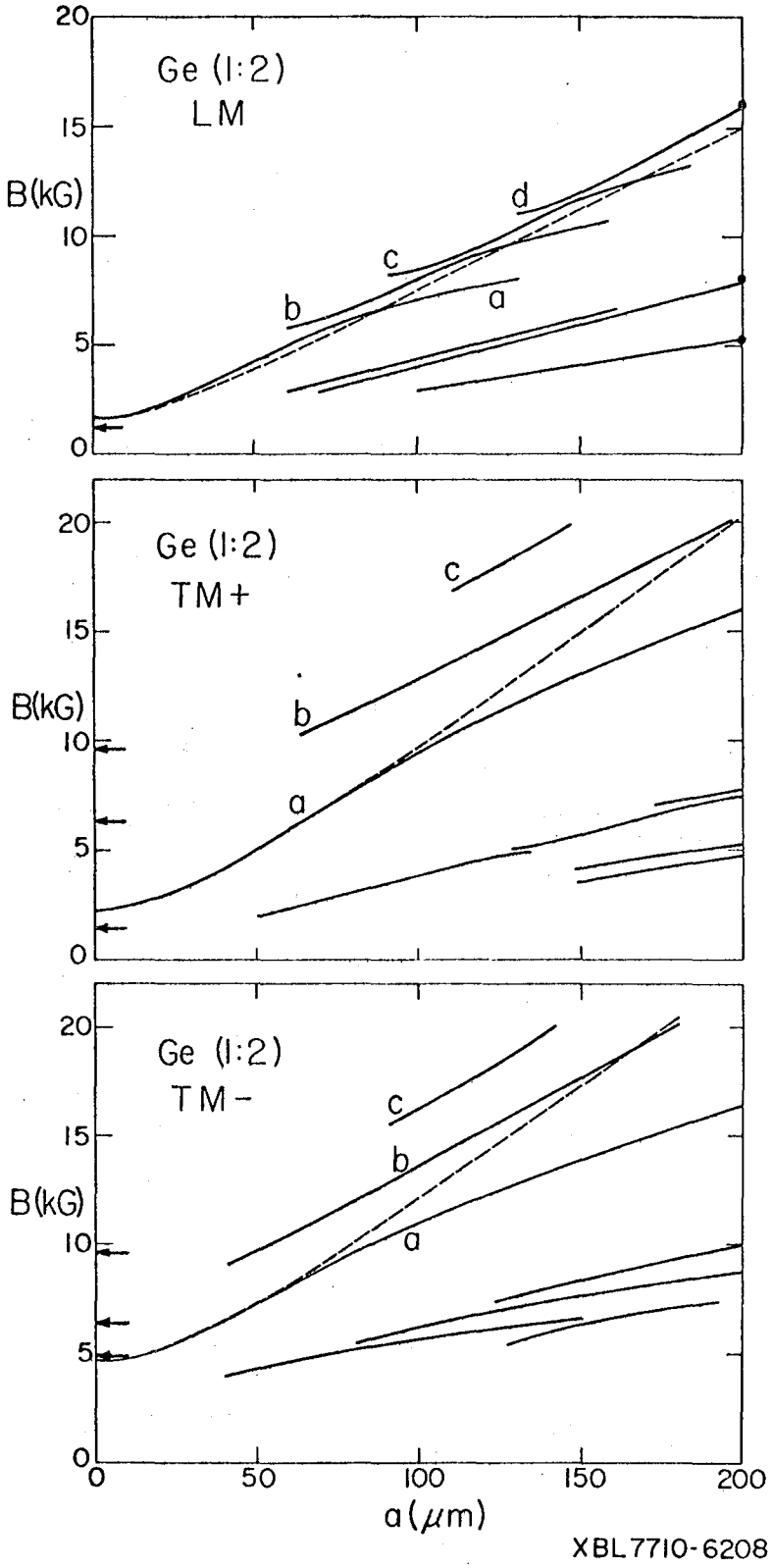
Ge (1:2)
LM
B(kG)
d
c
b
a
Ge (1:2)
TM+
B(kG)
c
b
a
Ge (1:2)
TM-
B(kG)
c
b
a
0
5
10
15
20
0
50
100
150
200
a(μm)
XBL7710-6208

Fig. 3

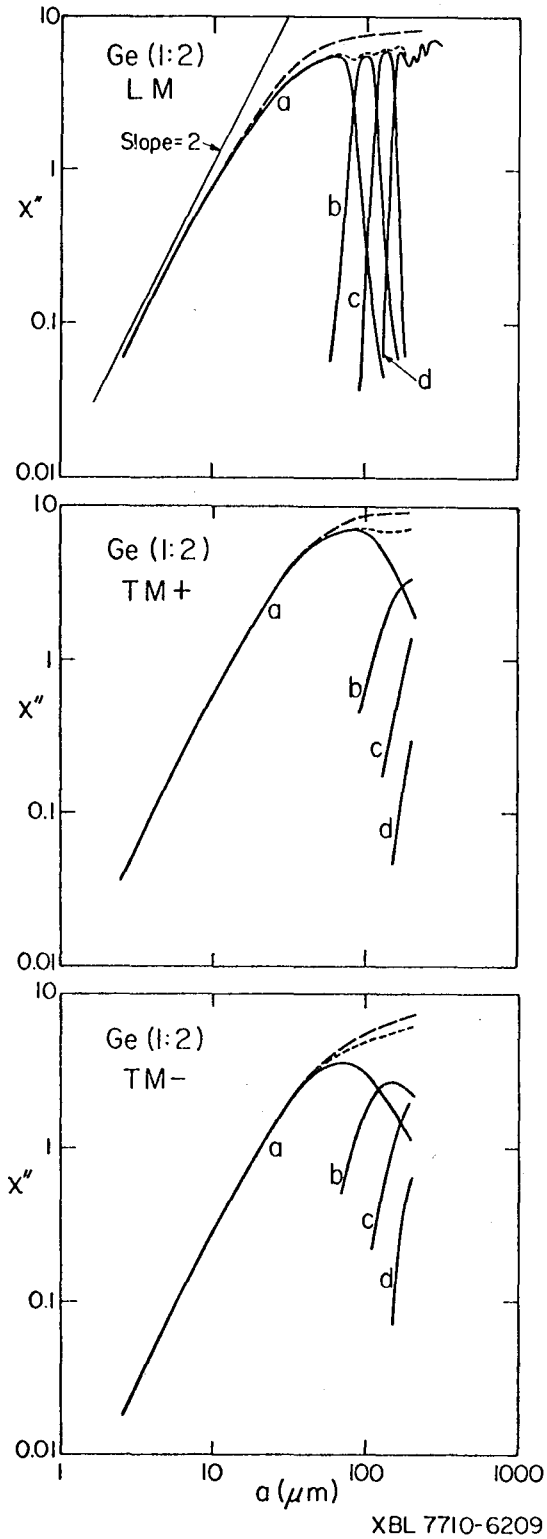

Fig. 4

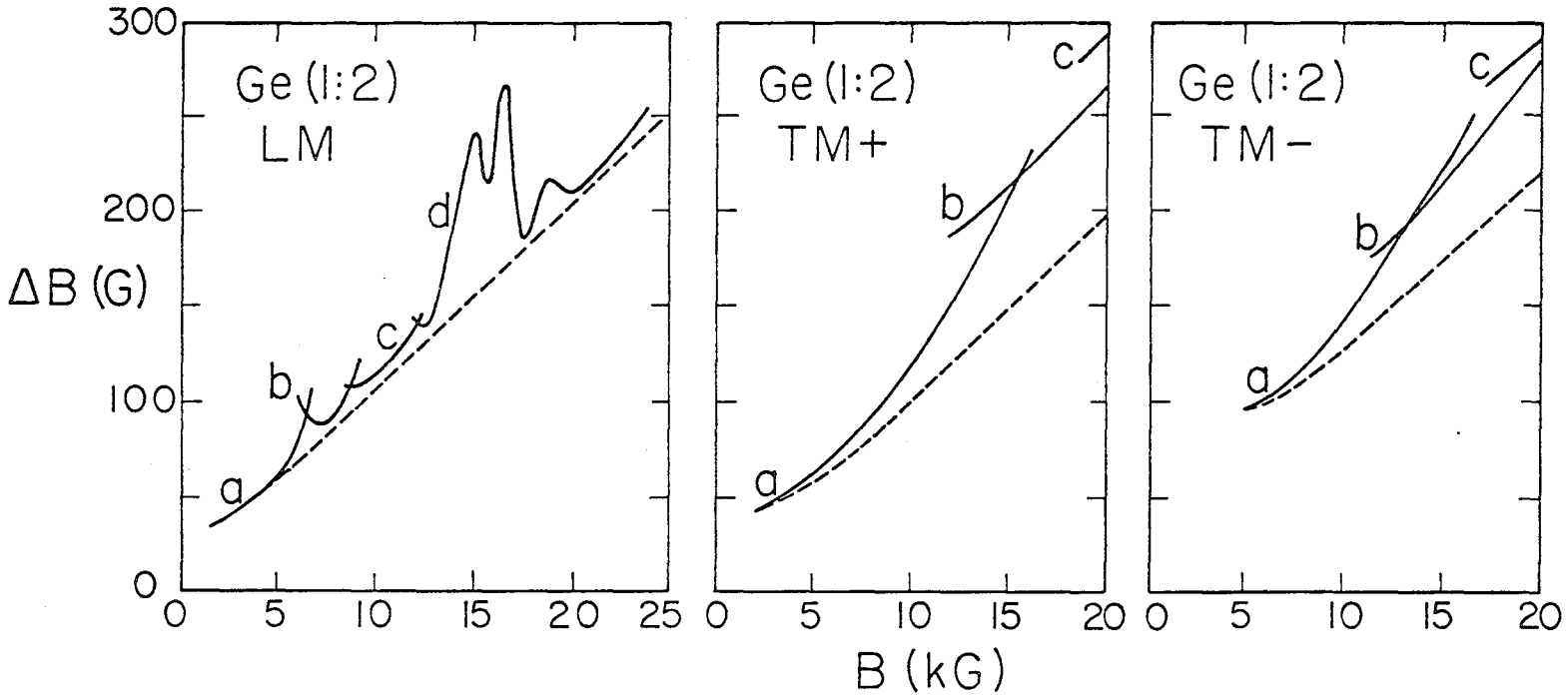

XBL 7710-6212

Fig. 5

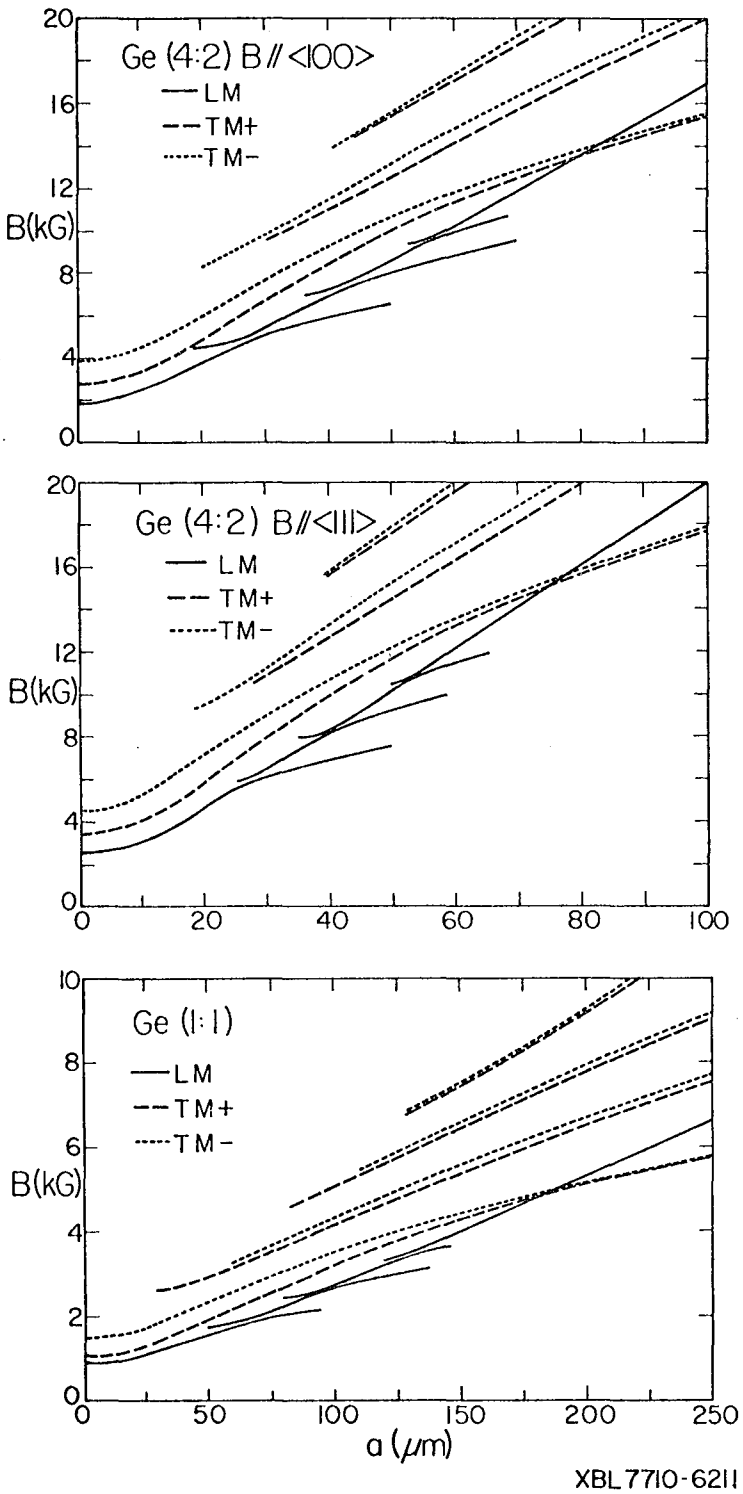

Fig. 6

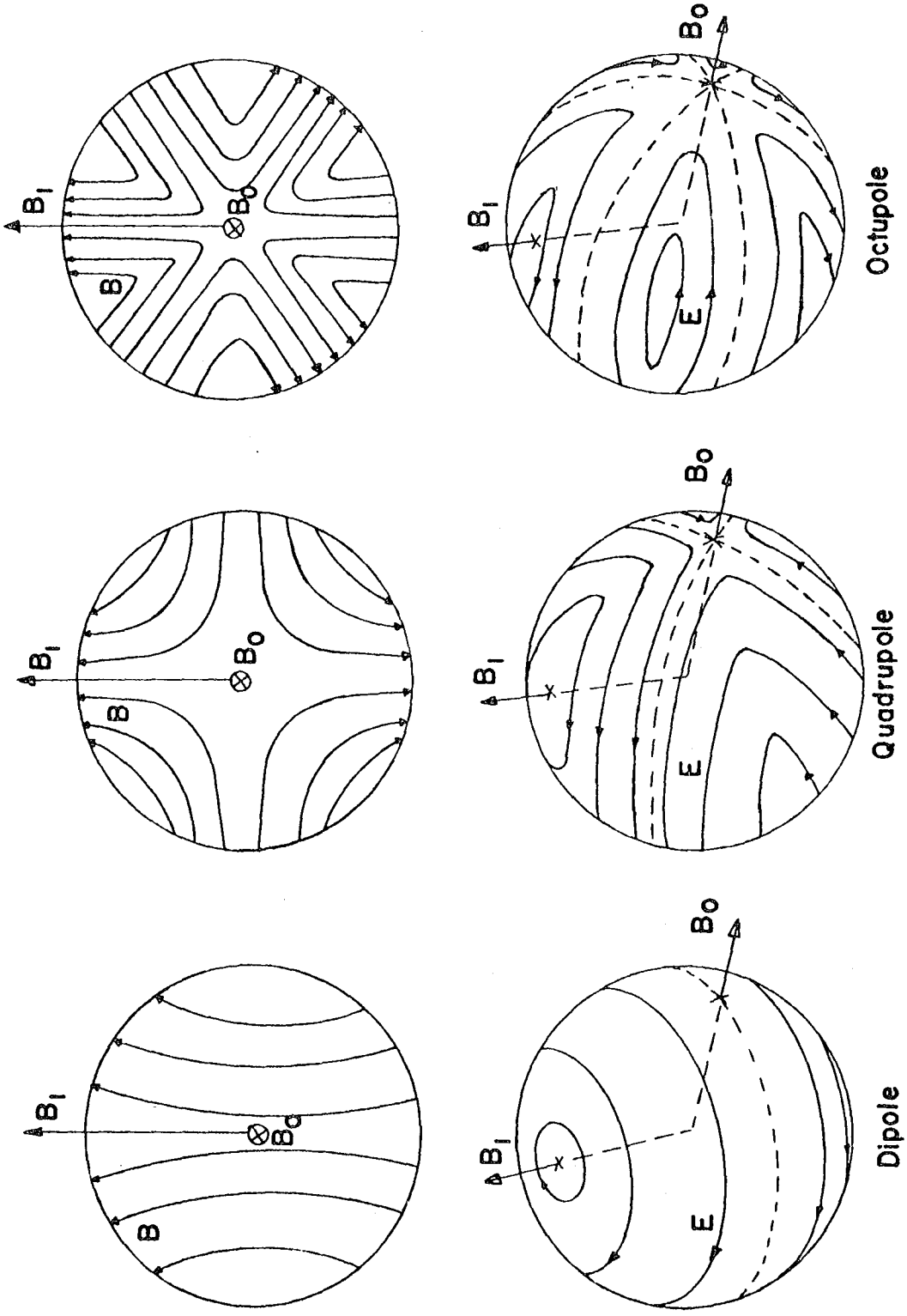

XBL 7710-10074

Fig. 7

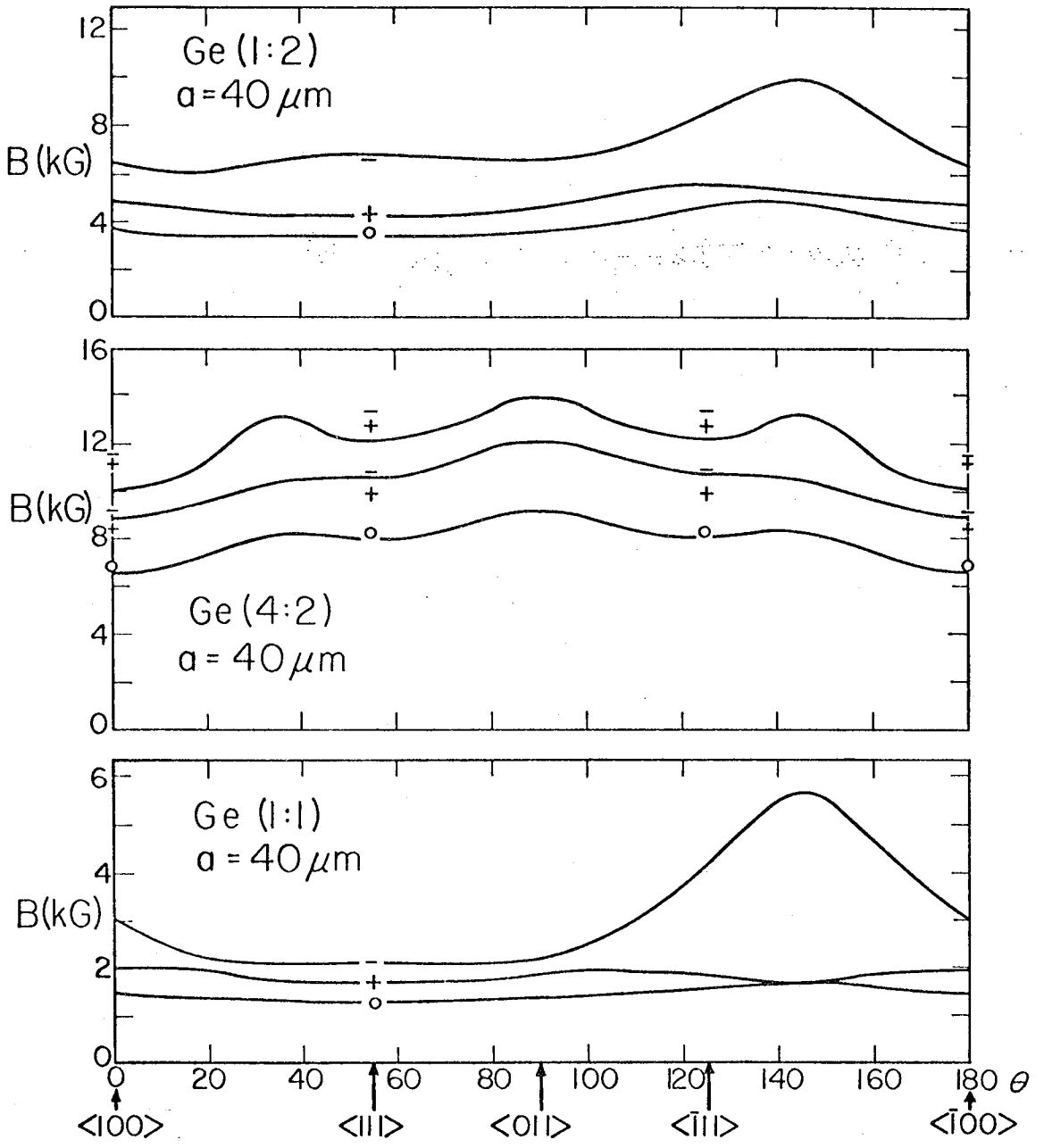

Fig. 8

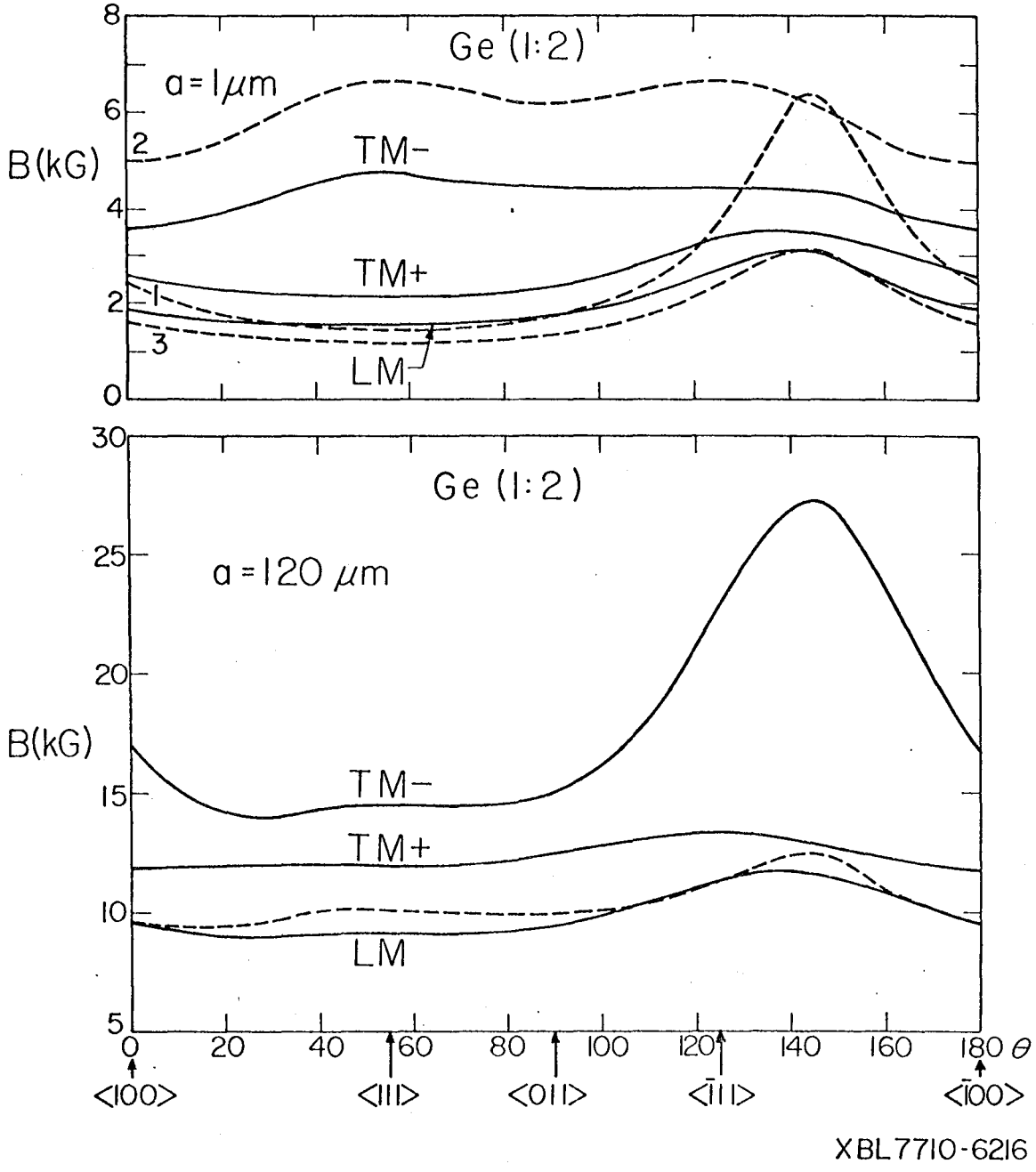

XBL7710-6216

Fig. 9

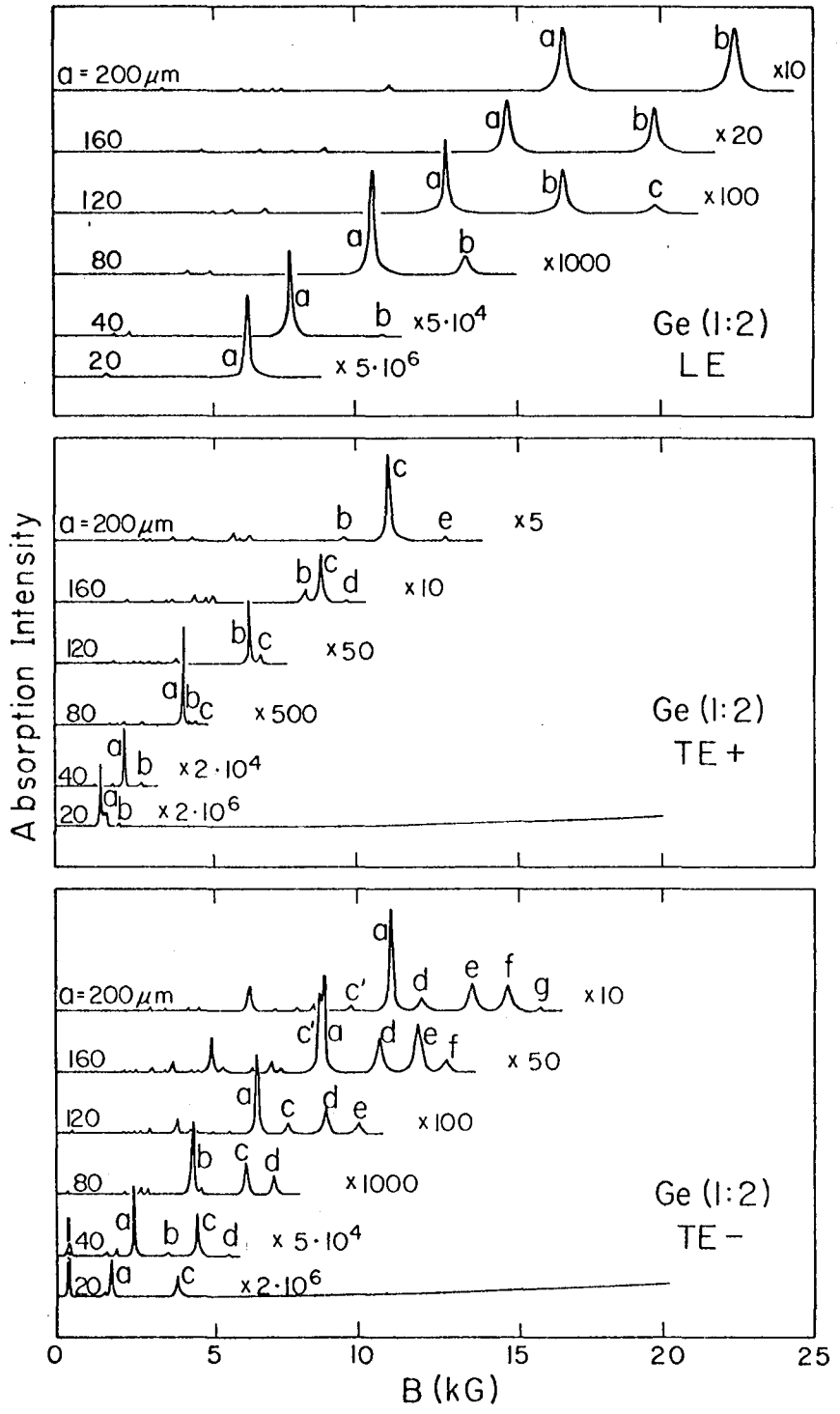

XBL7710-6213

Fig. 10

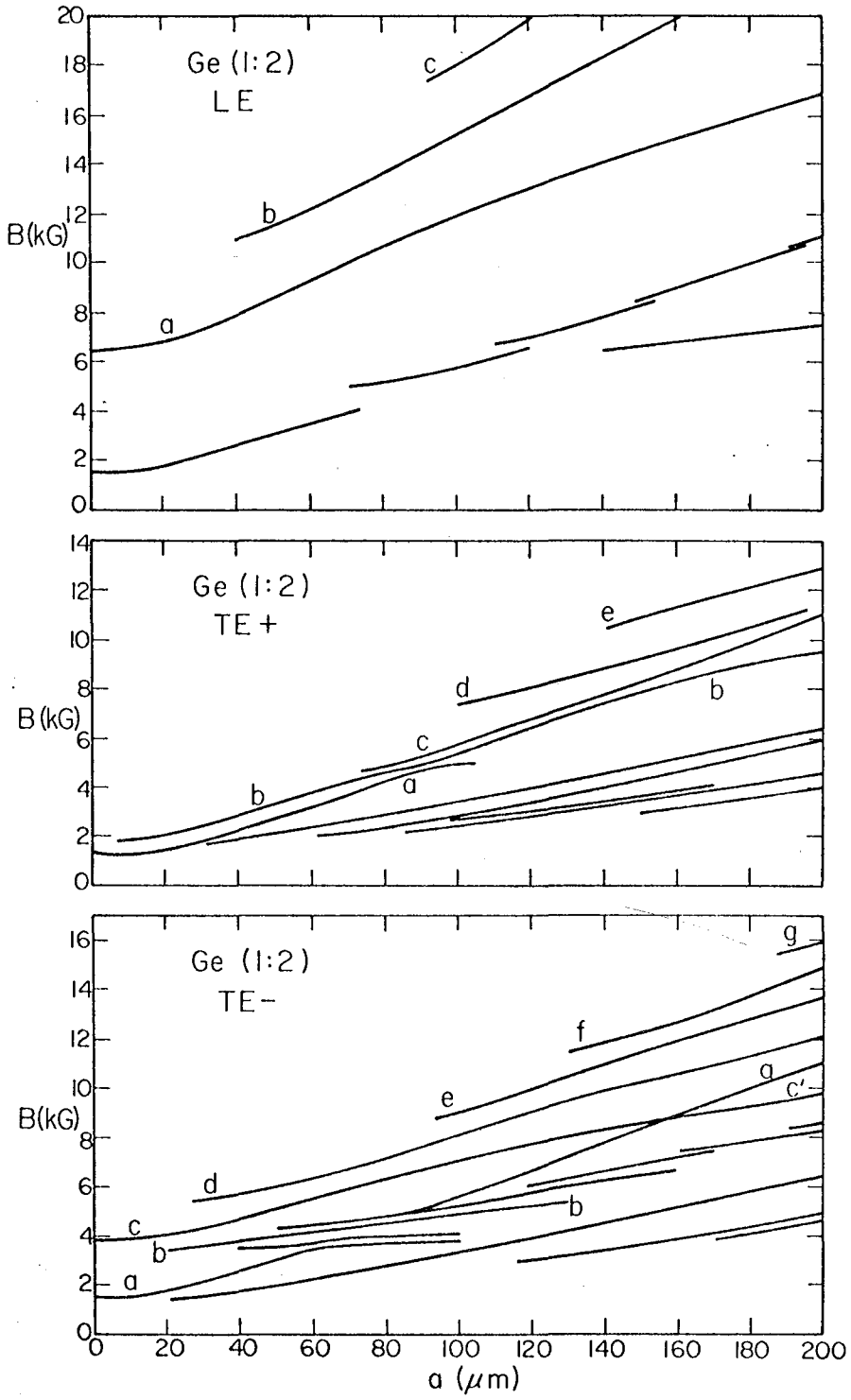

XBL 7710-6221

Fig. 11

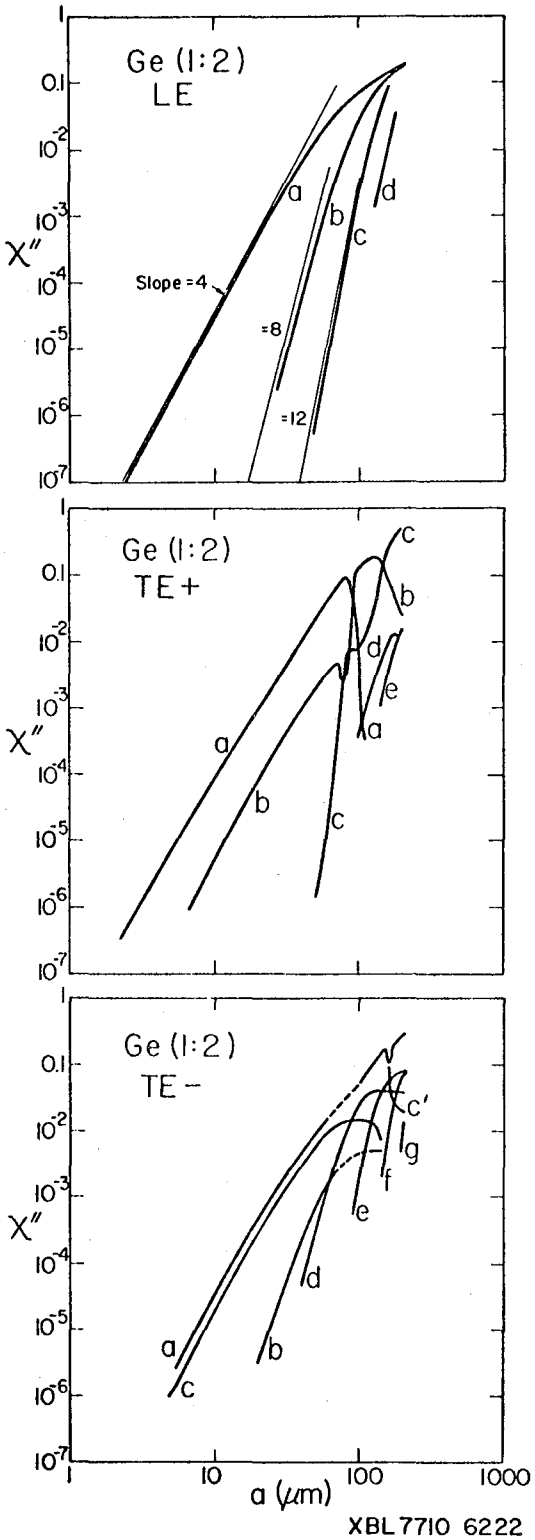

Fig. 12

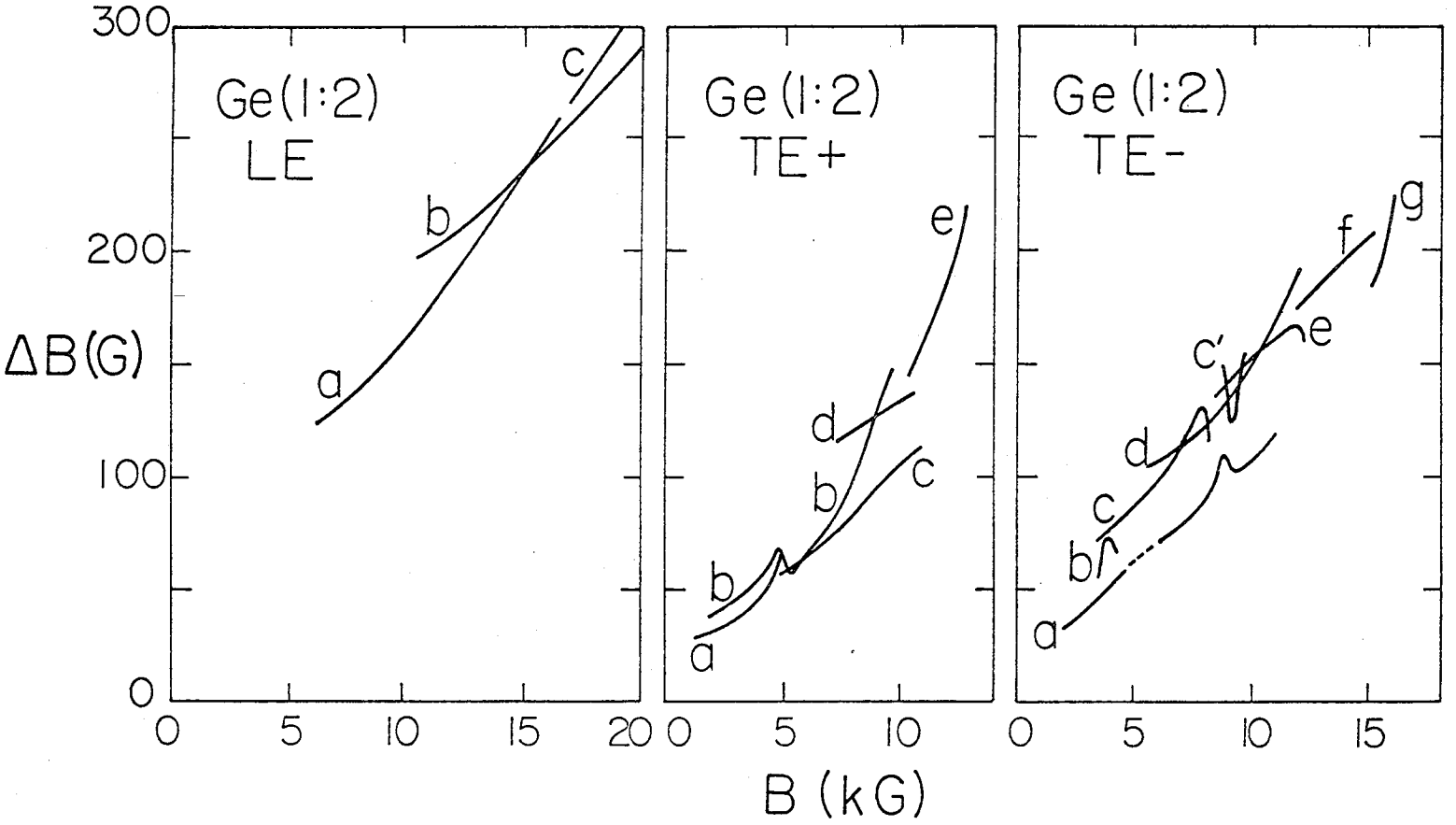

XBL7710-6214

Fig. 13

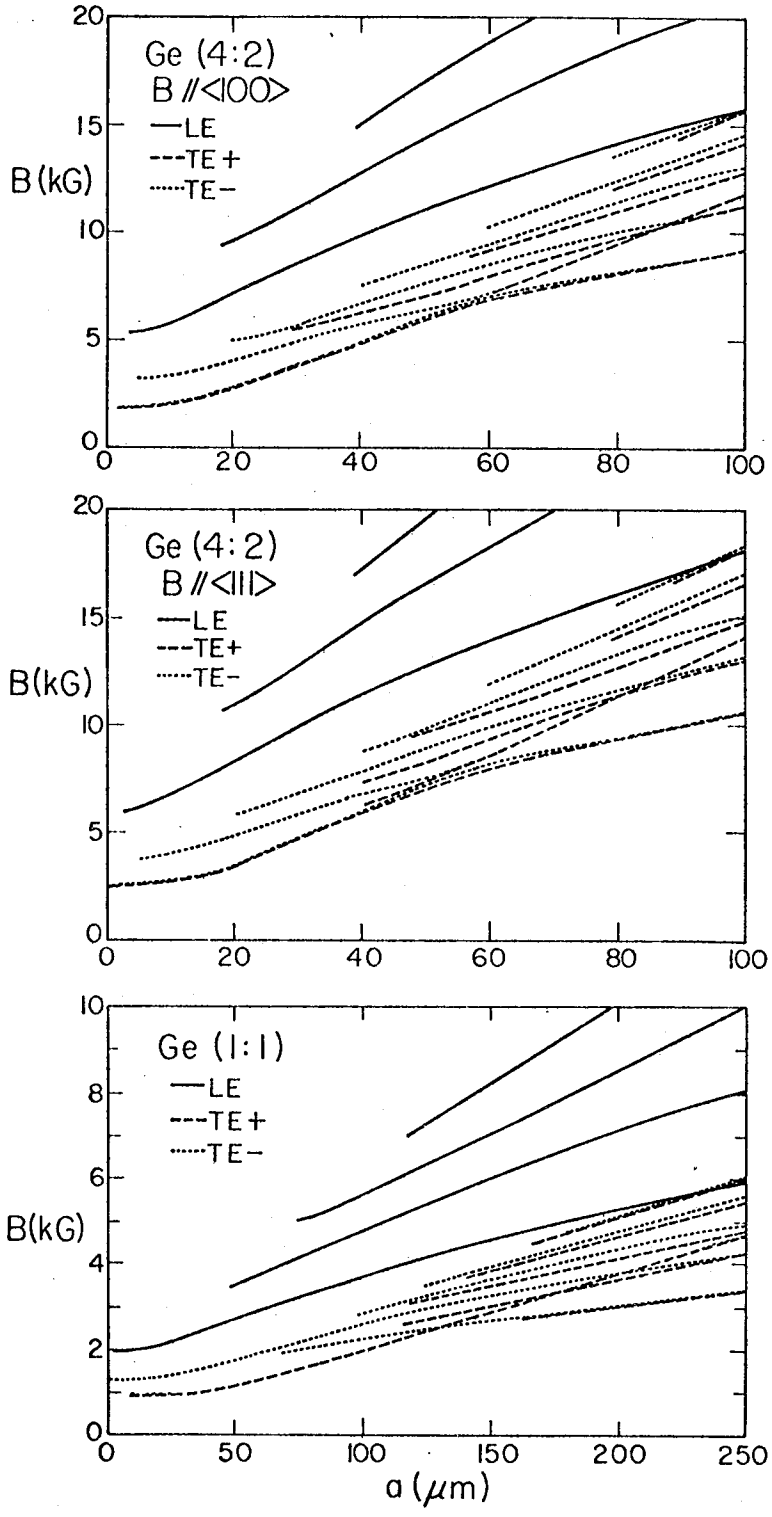

XBL 7710-6223

Fig. 14

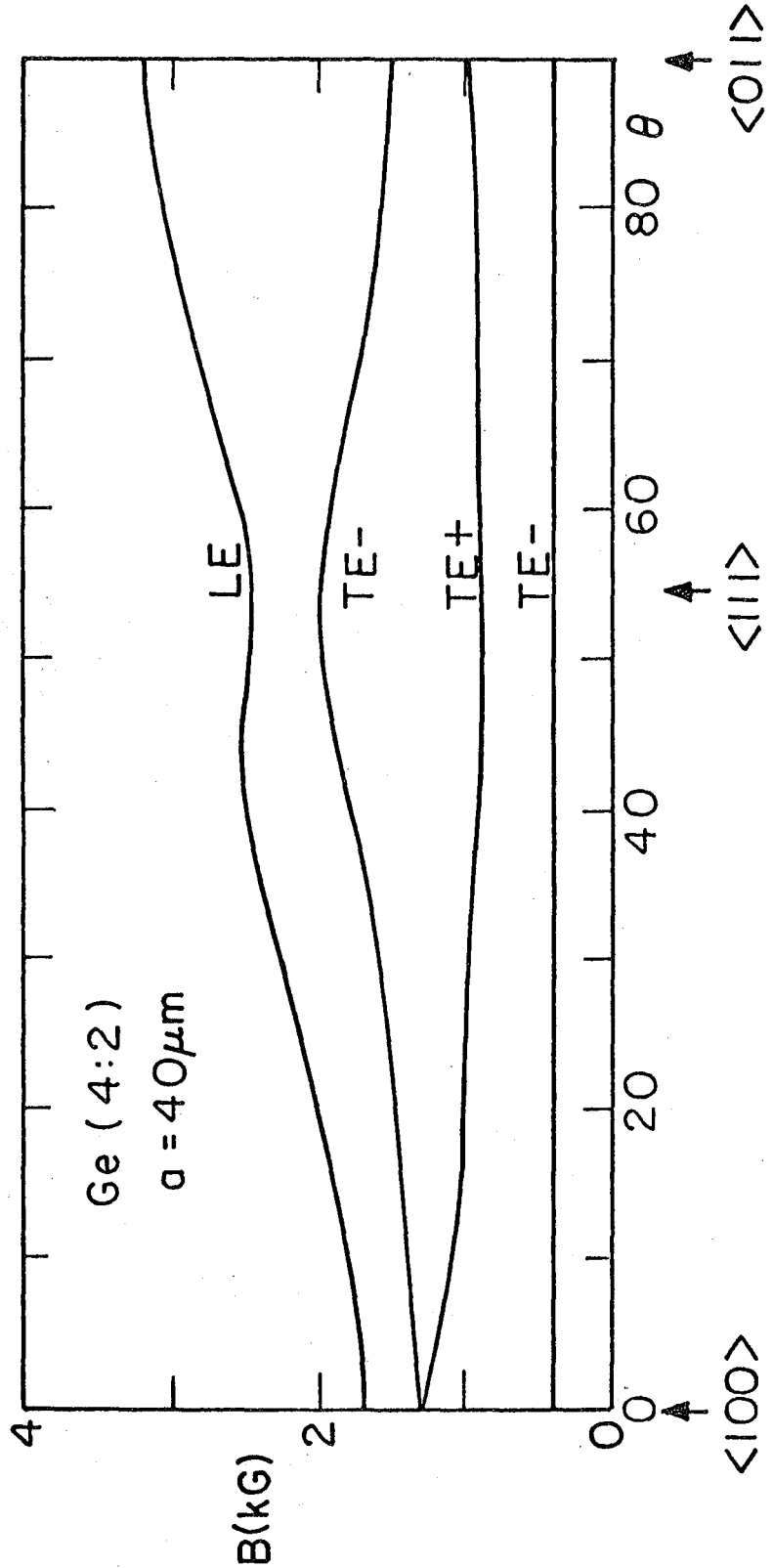
Ge (4:2)
a = 40μm
LE
TE-
TE+
TE-
B(kG)
4
2
0
0
20
40
60
80 θ
<100>
<111>
<011>
XBL7710-6220

Fig. 15

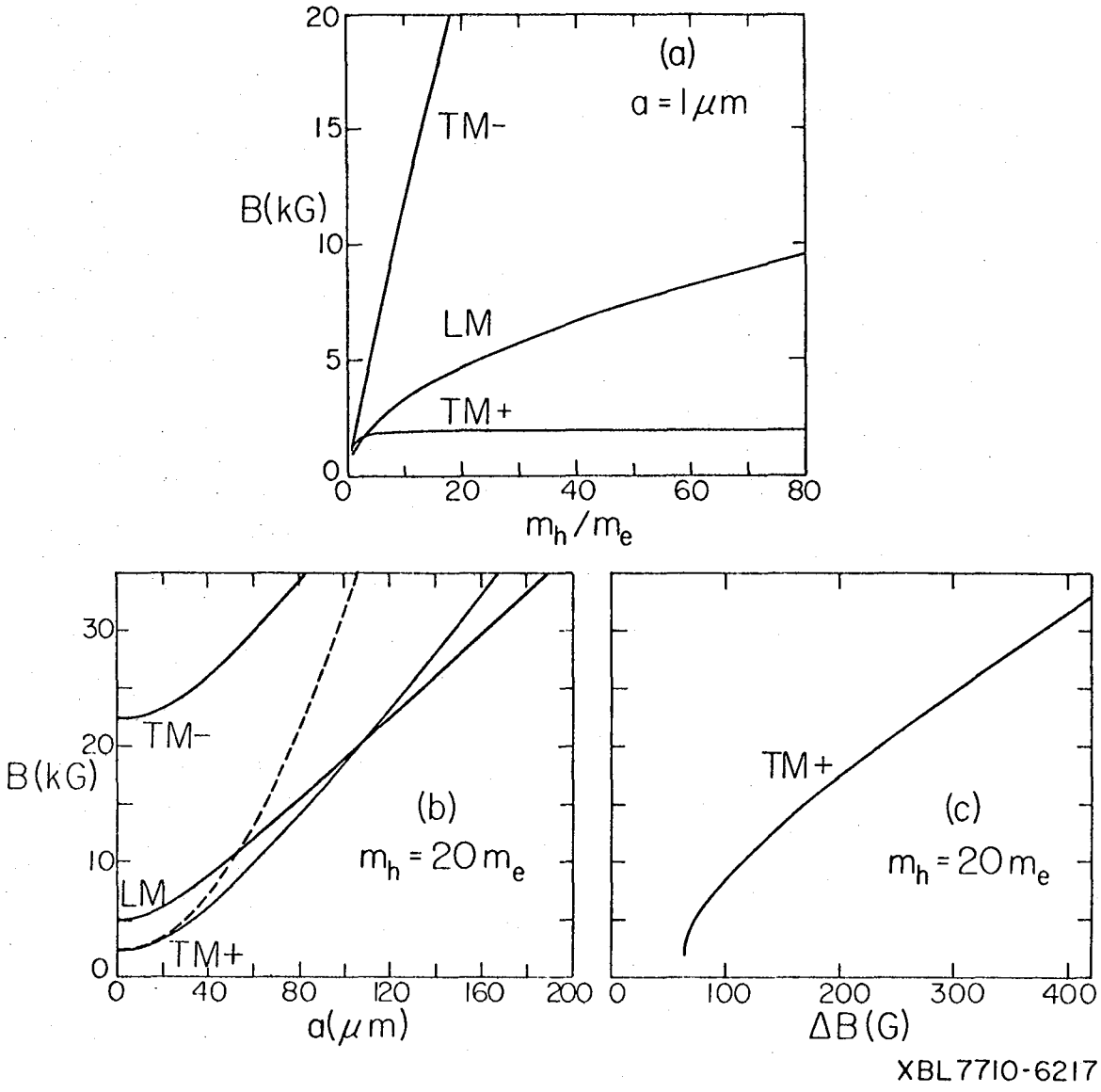

Fig. 16

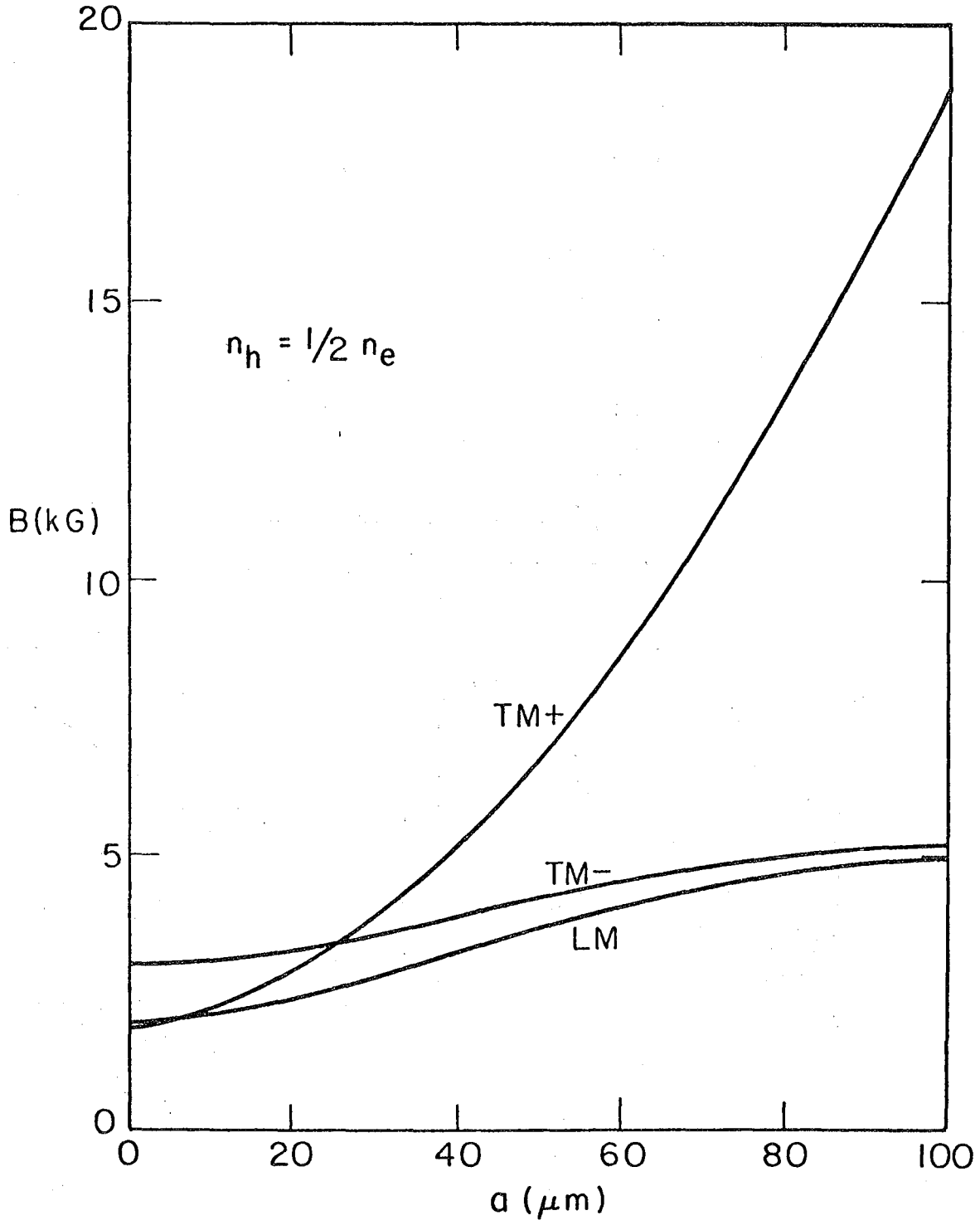

XBL7710-6219

Fig. 17

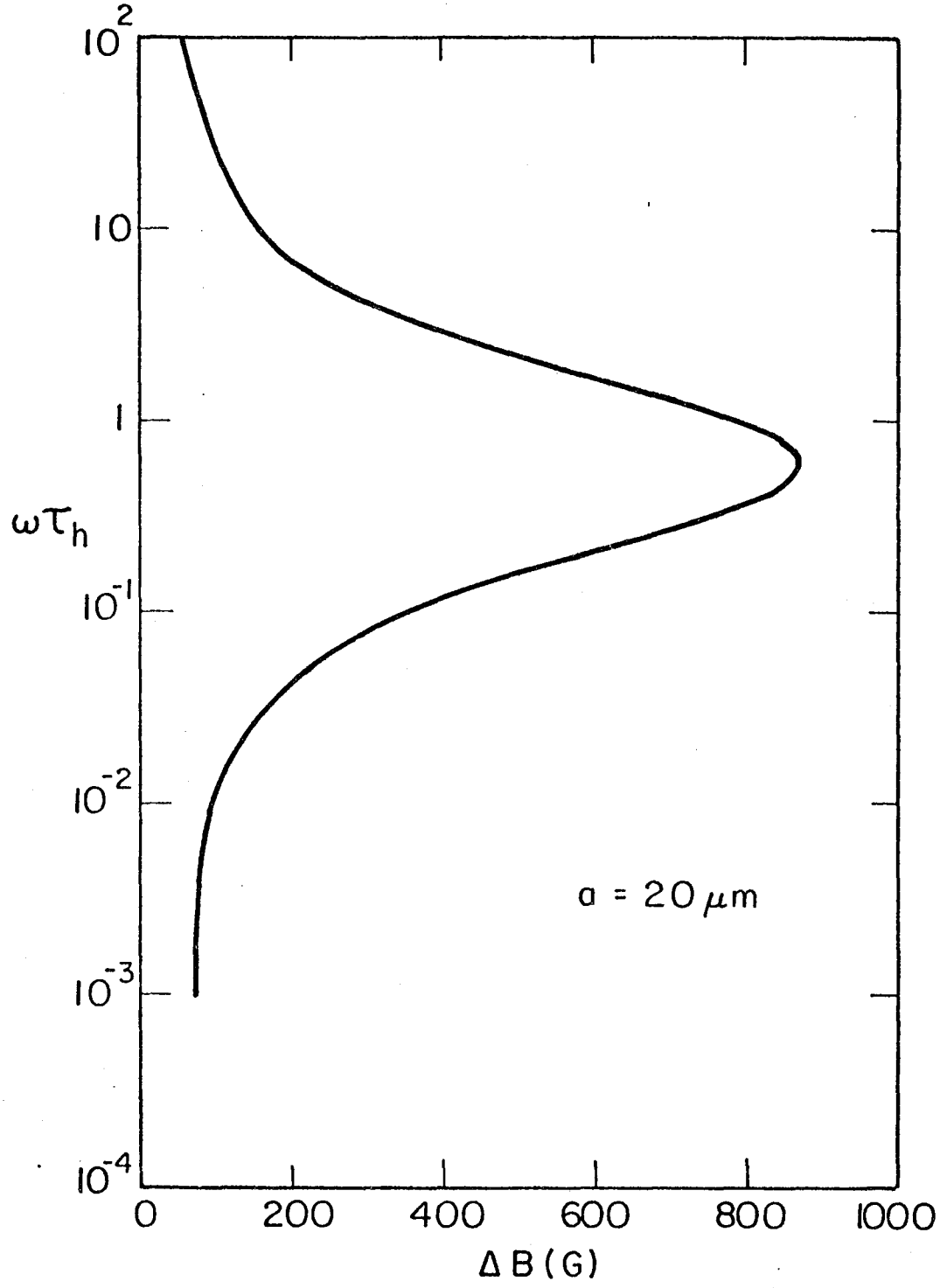

XBL 7710-6218

Fig. 18

This report was done with support from the United States Energy Research and Development Administration. Any conclusions or opinions expressed in this report represent solely those of the author(s) and not necessarily those of The Regents of the University of California, the Lawrence Berkeley Laboratory or the United States Energy Research and Development Administration.